AD-A130 755 BACKGROUND INFORMATION ON THE HE(3) NUCLEAR GYROSCOPE 1/1
(U) STANFORD UNIV CA W M FAIRBANK FEB 83
AFOSR-TR-83-0597 F49620-78-C-0088

UNCLASSIFIED F/G 17/7 NL

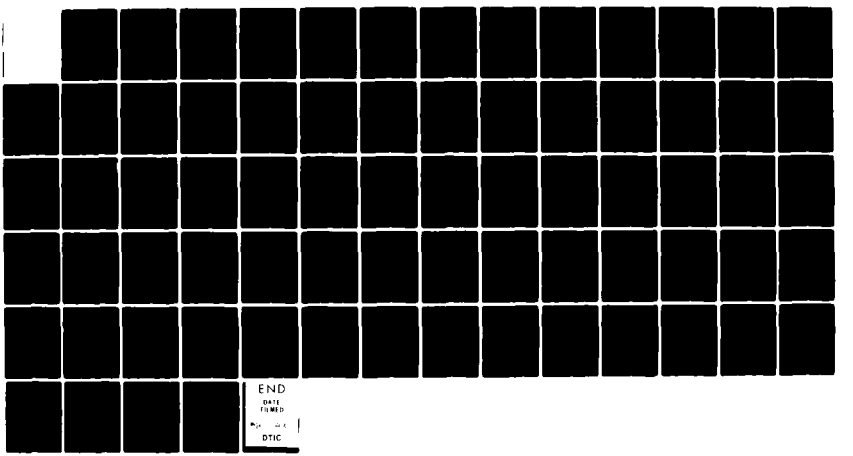

END
DATE FILMED
DTIC

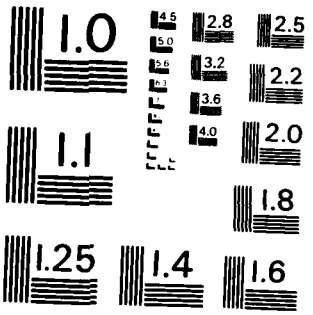

UNCLASSIFIED

SECURITY CLASSIFICATION OF THIS PAGE (When Data Entered)

REPORT DOCUMENTATION PAGE	READ INSTRUCTIONS BEFORE COMPLETING FORM
1. REPORT NUMBER AFOSR-TR- 83-0597 / 2. GOVT ACCESSION NO. AD-A130755	3. RECIPIENT'S CATALOG NUMBER
4. TITLE (and Subtitle) Final Scientific Report for AFOSR Contract # F49620-78-C-0088	5. TYPE OF REPORT & PERIOD COVERED Final Report 6/1/78 - 4/30/82
	6. PERFORMING ORG. REPORT NUMBER
7. AUTHOR(s) William M. Fairbank	8. CONTRACT OR GRANT NUMBER(s) Contact # F49620-78-C-0088
9. PERFORMING ORGANIZATION NAME AND ADDRESS Stanford University c/o Sponsored Projects Office Encina Hall Stanford, Ca. 94305	10. PROGRAM ELEMENT, PROJECT, TASK AREA & WORK UNIT NUMBERS 61102F 2305/B2
11. CONTROLLING OFFICE NAME AND ADDRESS USAF AFSC Air Force Office of Scientific Research/NE Bldg 410, Bolling AFB, D.C. 20332	12. REPORT DATE February 1983
	13. NUMBER OF PAGES 67
14. MONITORING AGENCY NAME & ADDRESS(if different from Controlling Office) Same	15. SECURITY CLASS. (of this report) UNCLASSIFIED
	15a. DECLASSIFICATION/DOWNGRADING SCHEDULE

16. DISTRIBUTION STATEMENT (of this Report)

17. DISTRIBUTION STATEMENT (of the abstract entered in Block 20, if different from Report)

Same as above

18. SUPPLEMENTARY NOTES

19. KEY WORDS (Continue on reverse side if necessary and identify by block number)

Introduction and Background; Low Temperature He^3 Nuclear Gyro; Experimental Results; Summary and Conclusions

20. ABSTRACT (Continue on reverse side if necessary and identify by block number)

During the contract period, the background necessary to proceed with the assembly and testing of the precision He^3 nuclear gryoscope was completed. This background work included experiments on He^3-He^4 liquid and gas mixtures in a prototype apparatus which was modified to provide additional information useful to the He^3 gyroscope research program. The precision quartz He^3 gryoscope was designed, constructed and delivered during this period as were the components of the airlock and cryostat probe assembly. A new ultra-low magnetic field was made which acheived 2 x 10-8G over the volume necessary for the (con't)

DD FORM 1 JAN 73 1473 EDITION OF 1 NOV 65 IS OBSOLETE S/N 0102-LF-014-6601

UNCLASSIFIED

SECURITY CLASSIFICATION OF THIS PAGE (When Data Entered)

20. Con't)

He^3 gyroscope. This not only exceeds the nominal requirements of the He^3 gyroscope, but is the lowest magnetic field region ever made. An engineering Ph.D. thesis was completed by Captain Gerald Shaw, working with Professor Daniel DeBra, on a theoretical analysis of the cross-axis response of a three-axis He^3 gyroscope and on kinematic rectification on a nuclear gyro.

FINAL SCIENTIFIC REPORT

for

AFOSR Contract # F49620-78-C-0088

William M. Fairbank
Principal Investigator

Michael Taber
Associate Investigator

February 1983

TABLE OF CONTENTS

ABSTRACT

During the contract period the background necessary to proceed with the assembly and testing of the precision $He^{(3)}$ nuclear gyroscope was completed. This background work included experiments on $He^{(3)}$-$He^{(4)}$ liquid and gas mixtures in a prototype apparatus which was modified to provide additional information useful to the $He^{(3)}$ gyroscope research program. The precision quartz He^{3} gyroscope was designed, constructed and delivered during the period as were the components of the airlock and cryostat probe assembly. A new ultra-low magnetic field shield was made which achieved 2×10^{-8} G over the volume necessary for the He^{3} gyroscope. This not only exceeds the nominal requirements of the He^{3} gyroscope, but is the lowest magnetic field region ever made. An engineering Ph.D. thesis was completed by Captain Gerald Shaw, working with Professor Daniel DeBra, on a theoretical analysis of the cross-axis reponse of a three-axis He^{3} gyroscope and on kinematic rectification in a nuclear gyro.

I. Introduction and Background

The department of physics and aeronautics-astronautics of Stanford University have undertaken the development of a uniquely stable He^3 nuclear gyroscope based on low-temperature technology. This development effort makes use of experience we have already obtained in techniques of polarizing He^3 by optical pumping, obtaining long He^3 nuclear relaxation times, obtaining low-magnetic-field regions in superconducting shields and selecting magnetically clean materials for use in these low-field environments, testing and working with precision fused quartz gyro assemblies and using SQUID magnetometry for gyro readout. Funding for the previous work has been provided on large part by AFOSR and NASA.

Prior to the current AFOSR funding, a crude prototype of the cryogenic He^3 nuclear gyroscope (He^3NG) was built. Using this apparatus, He^3-He^4 mixtures were condensed into a 4^o K low-field region and the resulting processing magnetization was observed with a signal-to-noise ratio in excess of 10^3 by use of a SQUID magnetometer. Although this prototype was too flawed (in large part due to magnetic contaminants) to function as a gyro, it was found that 0.07% He^3 - liquid He^4 mixture had a relaxation time of 40 hours in a 1 cm diameter Pyrex cell when the effect of magnetic-gradient-induced relaxation was deducted. This result was dominated by wall-induced relaxation since the subsequent use of a solid H_2 wall coating increased this relaxation time to more than five days (140 hours). This last result is encouragingly close to the theoretically estimated maximum relaxation time under these conditions of 170 hours due to He^3 - He^4 dipolar interactions.

In addition to these experimental measurements, a general analysis of the characteristics of a He^3 NG based on current low-temperature technology was made for the purpose of evaluating its potential for use in a future nuclear electric dipole moment experiment. This analysis considered two possible modes of operation of the He^3 NG and the results of one of these analyses are presented in Section III. The details of both the theoretical analyses and the relaxation time measurements can be found in the Ph.D. thesis of M. A. Taber. A summary of the experimental results was also presented at the 15th International Conference on Low Temperature Physics and published in the Proceedings.

In 1978, work was begun with support from AFOSR on the development of a working precision cryogenic He^4NG. This work has resulted in a gyro housing design (Fig. 1). This design and its tolerance sp-cifications are the result of the elaboration of our previous general analysis plus additional analytical work. Because of our desire to investigate the possibility of ultimately using this instrument for a demanding physics experiment, design emphasis has been placed on a) magnetic field stability, b) long relaxation time, c) good readout resolution, and d) flexibility anf ease of modification. The housing was designed in collaboration with Mr. Don Davidson of Optical Instrument Design, Inc. who supervised the fabrication of the unit.

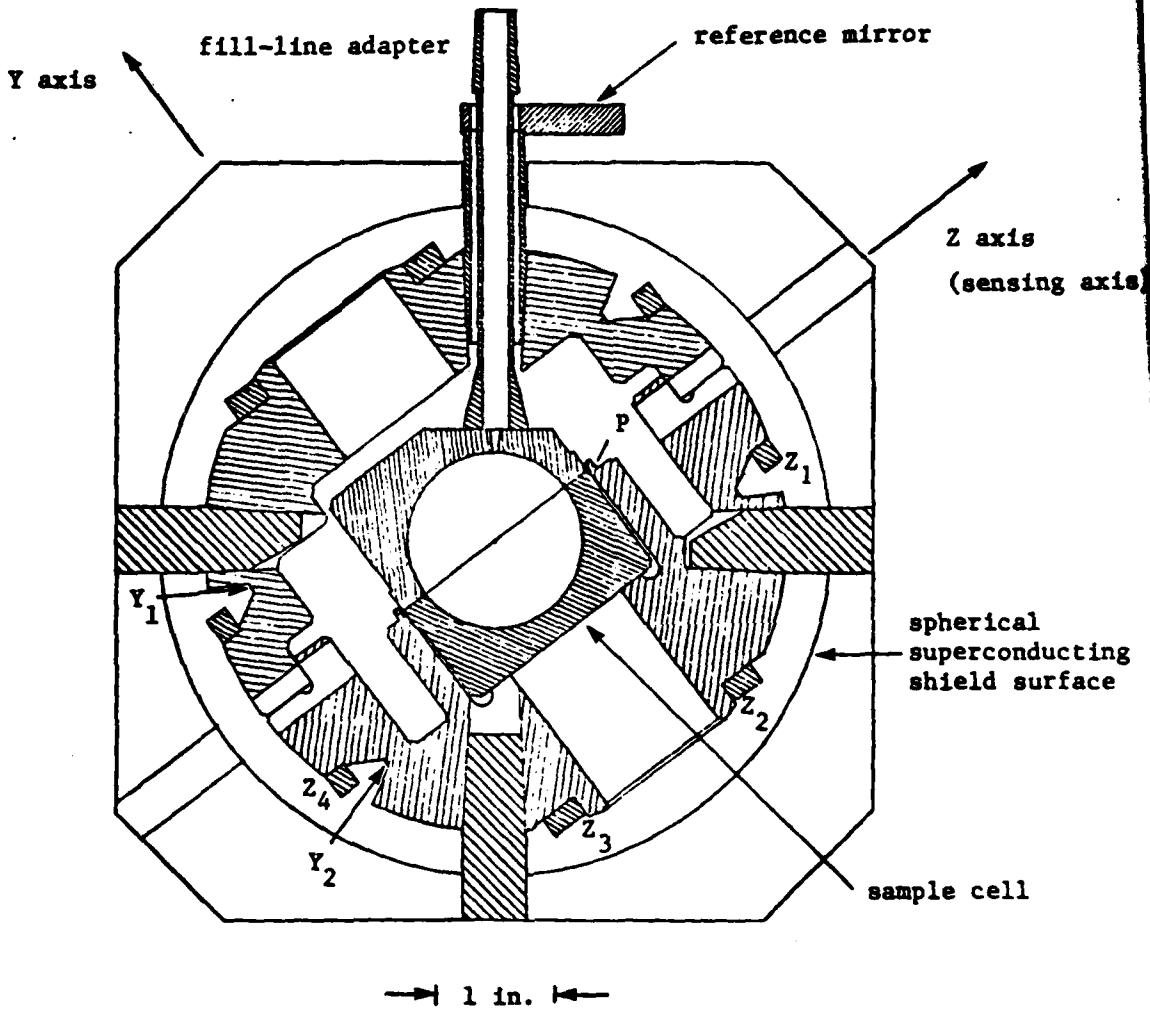

Fig. 1. Schematic cross sectional view of the He^3 gyro housing. Coil forms Z_1 - Z_4 are axially symmetric about the Z axis and are configured to generate the primary 6th-order field. Coils X_1, X_2(not shown) and Y_1, Y_2 are symmetric about the X and Y axes, respectively, and provide 4th-order fields for correction and initialization purposes. Coil P is the readout coil. Not shown is the valve assembly which resides in the fill-line adapter. All parts shown are fused silica.

II. Description of the Low Temperature He^3 Nuclear Gyro

It is a well-known result of quantum mechanics that the equations of motion of the expectation value of a nuclear magnetic dipole moment $\vec{\mu} = \gamma\hbar\vec{I}$, where $\hbar\vec{I}$ is the nuclear spin vector operator, are

$$d\langle\vec{\mu}\rangle/dt = \gamma\langle\vec{\mu}\rangle \times \vec{B} \qquad [1]$$

when the nucleus is placed in a magnetic field $\vec{B}$.[1] This of course, is formally identical to the classical equations of motion that would be obeyed by any freely spinning body that possessed a magnetic dipole moment aligned along its angular momentum vector. Another basic theoretical result is that in the case of spin-1/2 particles (such as the He^3 nucleus), there can be no higher multipole moment than the dipole.[2] Thus [1] represents the only external interaction that is necessary for us to consider.

If a large number of non-interacting He^3 atoms are collected in a sample volume and are subjected to a homogeneous magnetic field, then provided the components of the total angular momentum are large compared to $\hbar$, the motion of the total angular momentum can be treated classically. Thus we may replace the expectation values of the individual spin vectors in [1] with the classical variable $\vec{M}$, the sample magnetization:

$$d\vec{M}/dt = \gamma(\vec{M} \times \vec{B}). \qquad [2]$$

Equation [2] raises an intriguing question: is it possible to use such a collection of He^3 atoms to make a practical gyroscope? In order

to make a useful He^3 nuclear gyroscope (He^3NG), we must at least approximate the various conditions that were noted in arriving at equation [2], and additionally the magnetic environment must be strictly controlled. In practical terms, this means the following requirements must be met:[3] (1) A sample containing a large number of polarized, rapidly-diffusing He^3 atoms must be obtained. (2) The components of the magnetization must have usefully long relaxation times. (3) The polarized He^3 must be maintained in a spherical sample cell, and any nearby materials that have large magnetic susceptibilities (paramagnetic or diamagnetic) must also have at least cubic symmetry. (4) If there is to be relative motion between the sample magnetization and the gyro case, materials that can cause significant radiation damping must not be in close proximity to the sample. (5) A sensitive means of measuring the direction of the sample magnetization without perturbing the magnetization to an unacceptable degree must be provided. And finally, (6) the average magnetic field over the sample volume (exclusive of that due to the sample itself) must either be intrinsically stable or independently measured and controlled with sufficient stability. In view of the relaxation time requirement in (2), it is also important that the magnetic field gradients be kept small.

There are at least two ways in which a He^3NG might be formulated. One way would be to reduce the average magnetic field over the sample volume to zero. In this case, it can be seen from equation [2] that $\vec{M}$ should remain fixed in direction, and rotation of the gyro housing about any axis orthogonal to $\vec{M}$ could be measured. Although this approach has the advantage of two-axis sensitivity, an analysis of its potential performance (as implemented by low temperature techniques) indicates that in

most respects it will be inferior to the alternative approach.[4]

The alternative approach is to apply a very constant, uniform magnetic field $\vec{B}_o = B_o\hat{k}$. By letting $\omega_o = -\gamma\vec{B}_o$ ($\gamma = -2.04 \times 10^4$ rad sec^{-1} G^{-1} for He^3) equation [2] can be written in this case

$$d\vec{M}/dt = -(\vec{M} \times \omega_o). \qquad [2']$$

Equation [2'] is readily solved by the classical technique of taking the time derivative of $\vec{M}$ in another frame that is rotating with respect to the inertial frame with angular velocity $\vec{\Omega}$:

$$(d\vec{M}/dt)_{inertial} = (d\vec{M}/dt)_{rot} + \vec{\Omega} \times \vec{M} ,$$

thus

$$(d\vec{M}/dt)_{rot} = \vec{M} \times (\vec{\Omega} - \vec{\omega}_o). \qquad [3]$$

Equation [3] shows that $\vec{M}$ is stationary in the frame that is rotating with angular velocity $\vec{\omega}_o$ irrespective of the orientation of $\vec{M}$ with respect to $\vec{B}_o$. (Of course, M_z is a constant of the motion.) Thus $\vec{M}$ precesses about the z axis at the Larmor precession frequency $\vec{\omega}_o$ with respect to inertial space.

We now consider the field sources of $\vec{B}_o$ to be fixed with respect to the gyro case and ask what happens when the gyro case is rotated with respect to the inertial frame. If the case is rotated at a rate $\vec{\Omega} = \Omega\hat{k}$ we see by comparing [2'] and [3] that the precession frequency, as measured in the frame of the gyro case is shifted by an amount

$$\delta\omega_o = \Omega . \qquad [4]$$

By integrating [4] with respect to time we also see that if the case is rotated about the z axis by an angle $\Delta\phi$, then the Larmor phase will also shift the same amount. Thus, by initially establishing $\vec{M}$ in the x-y plane and continually monitoring the phase of M_x (or M_y), rotations about the z axis can be measured. It is clear, however, that since ω_o is not fixed by any constant of nature, its phase and frequency must be initially established by measurement when the gyro case is mounted on an inertial platform or is at least subjected to an accurately known rate of rotation.

Now if the case is rotated about the x or y axis with a velocity $\vec{\Omega}$ such that $|\vec{\Omega}| << |\omega_o|$, then it is seen from [3] that in the frame of the gyro case, $\vec{M}$ will precess about $\vec{\omega}_o - \vec{\Omega}$ at a rate $\omega_o[1 + O(\Omega/\omega_o)^2]$. Thus $\vec{M}$ will "adiabatically follow"[1] $\vec{B}_o$ with only a second order shift in the Larmor frequency. This approach therefore yields a single-axis gyroscope which is limited to rotation rates that are small compared to ω_o. It is this type of gyroscope that we will now discuss in greater detail within the context of low temperature techniques.

The low temperature He^3HG is depicted schematically in Fig. 2. Although low temperature techniques introduce certain complications, they offer two significant advantages to the He^3NG. The first is that the flux-quantization property of type I superconductors means that the applied field is intrinsically stable except for two effects that will be discussed below: the variation of dimensions and penetration depth with temperature. This stability makes it unnecessary to independently monitor the magnetic field.

The other advantage is that a SQUID (Superconducting Quantum Inter-

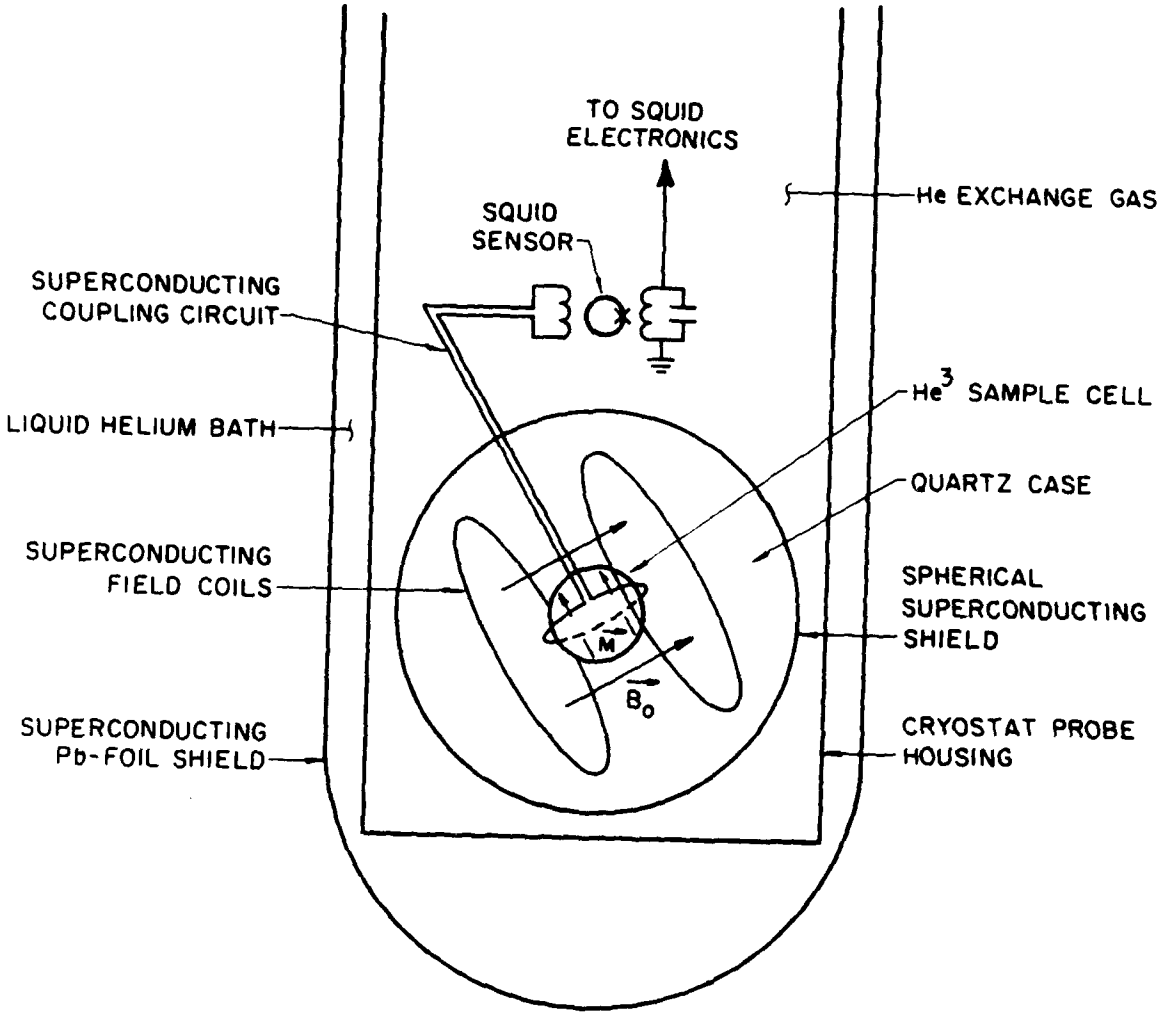

Fig. 2. Schematic of ^{3}He nuclear gyroscope

ference Device) magnetometer can be used for readout. This device can be coupled to the sample magnetization with a superconducting circuit. The output of the magnetometer is fed back into this circuit so that the reaction currents that would normally flow due to motion of the sample magnetization are reduced by a factor equal to the loop gain of the magnetometer. This readout technique, then, utilizes the high sensitivity of the SQUID for accurate readout and at the same time minimizes the effect of the coupling circuit on the sample magnetization.

For the purposes of discussion we will now describe a possible version of the low temperature He^3NG in some detail. The values of the various parameters that are specified here form the bases for the estimates of the gyro performance that will be quoted later. It should be noted that the choices of parameter values were based on (a) reasonable compromises between various tradeoffs, although certain applications may require different compromises than those selected here; (b) capabilities of our current optical pumping and low temperature laboratory equipment; and (c) laboratory experience using techniques that are similar (if not identical) to those that are proposed here.

The He^3NG that is being contemplated consists of a fused quartz housing with a 3.8 cm diameter sample cell that has been tumble lapped and assembled to maintain a sphericity of $\pm$ 0.13 μm. Permanent leak-tight assembly is achieved by optical contacting. The housing includes as integral elements the pickup loop for the magnetometer, field coils, and a 15 cm diameter spherical superconducting shield on the outer surface. Because all of the conductors in the quartz housing are to be superconducting and therefore perfectly diamagnetic, they must either be

physically small or arranged to maintain cubic symmetry if excessive precession of the sample magnetization is to be avoided.

The quartz housing is to be located in a cryostat probe that can be cooled to 4.2 K by lowering into a dewar that is lined with a degaussed superconducting lead-foil shield. This shield is degaussed by use of an iterative expansion technique that has been perfected in our laboratory,[5] and can be expected to provide a low-field region with a magnetic field of $\sim 5 \times 10^{-8}$ G. It is estimated that this field should have a gradient on the order of 10^{-8} G cm^{-1} in the center. If the spherical gyro shield is carefully cooled in this ambient field, it will trap a field of similar magnitude and configuration.

In our analysis, we have assumed a value for the Larmor frequency of $\omega_o = 1$ rad sec^{-1} ($B_o = 5 \times 10^{-5}$ G). This number is primarily constrained by magnetic gradient-induced spin relaxation considerations (see below). It would be possible to increase ω_o significantly with no degradation of gyro performance or reduction of dimensional tolerance requirements if the diameter of the gyro housing (i.e., the spherical shield) were made larger.

The He^3 can be polarized at room temperature using optical pumping[6] and admitted to the sample cell via a glass filling tube. A mechanical closure in the form of a tapered quartz plug can be opened to admit the sample and then closed to prevent diffusion in and out of the sample cell. Based on our experience with the condensation of polarized He^3 - He^4 mixtures, it is estimated that if the He^3 is polarized to 10% at room temperature it will have $\sim$ 2% initial polarization in the sample cell. If it is required that the initial internal magnetic-flux density be 3×10^{-6}G, then a He^3 density of 3×10^{-6} mol cm^{-3} is necessary in the sample cell.

It will undoubtedly be essential that a cryogenic wall coating of solid H_2 be used in order to reduce wall-induced nuclear relaxation of the He^3.[7] It is possible that a certain amount of He^4 gas could be used to reduce further wall-induced relaxation as will be discussed below.

The last element that must be specified in order to estimate the He^3 NG performance are the noise and drift characteristics of the SQUID For this purpose we have used the Clarke, Goubau, and Ketchen (CGK) data on dc tunnel-junction SQUIDs.[8] It should be noted, however, that the dc tunnel-junction SQUIDs are still only laboratory devices and are not yet commerically available. Currently we are using rf-biased hybrid SQUIDs which have a noise level approximately three times higher than the CGK result when referred to the input.

Having described a possible low temperature He^3NG, we will now summarize the results of our estimates of three important performance parameters based on this description: (1) He^3 nuclear relaxation time, (2) readout resolution, and (3) stability of the Larmor frequency, i.e., drift and precession effects.

1. He^3 Nuclear Relaxation Time

The relevant relaxation time is T_2, the transverse relaxation time.[1] There are three significant relaxation mechanisms: intrinsic relaxation, wall-induced relaxation, and relaxation due to magnetic field gradients. In the first two cases $T_2 = T_1$, the longitudinal relaxation time. In the case of relaxation due to field gradients, however, T_1 and T_2 are not generally equal, although in the present case they should be of the same order of magnitude.

Both intrinsic and gradient-induced relaxation are relatively well-understood. In the case of intrinsic relaxation, the relaxation rate of pure He^3 gas is given approximately by[9]

$$T_I^{-1} \simeq 2\gamma^4\hbar^2 I(I+1)(\pi\beta m)^{\frac{1}{2}} n_3 d^{-2} \qquad [5]$$

where $I = \frac{1}{2}$ is the nuclear spin quantum number, $\beta = (kT)^{-1}$, n_3 is the He^3 number density, and d is the atomic hard-core diameter. We note that of the controllable parameters in equation [5], β and n_3, n_3 is the most important. Under the proposed conditions for the He^3NG, [5] yields the estimate $T_1 \simeq 7 \times 10^6$ sec $\simeq$ 80 d.

The expressions for nuclear relaxation due to diffusion through magnetic field gradients[10] are not particularly difficult to obtain but are quite cumbersome for an arbitrary field configuration. For simplicity, we will limit the present discussion to the case of a uniform field plus an axially symmetric uniform gradient: $\vec{B}(\vec{r}) = B_o\hat{k} + g(2\hat{i}x - \hat{j}y - \hat{k}z)$. In this case

$$T_{2G}^{-1} \leq 0.16\gamma^2 g^2 R_o^4 D^{-1} \qquad [6]$$

where D is the He^3 diffusion coefficient and T_{2G}^{-1} is the transverse relaxation rate due to the gradient g. For the proposed He^3 density $D \simeq 1$ cm^2 sec^{-1}, and we estimate $T_{2G} \simeq 10^7$ sec. This is obtained with the assumption that $g \simeq 10^{-8}$ G cm^{-1}. It is important that care be taken to avoid ferromagnetic contaminants near the sample volume.[11,4]

In the case of wall-induced relaxation, the situation is not so certain. The only data that appear to be available of He^3 relaxation measurements with a solid H_2 wall coating are the T_1 measurements of Barbé, Laloë, and Brossel[7] (BLB), and our T_1 measurements.[4] The BLB measurements were made with a He^3 density $\sim 10^{-2}\times$ that being proposed here. They obtained a relaxation time (T_1) of 60 hours in a 3 cm diameter

cell that was completely dominated by wall-induced relaxation. Our results, on the other hand, were obtained with a He^3 density ~ 7× that being presently considered and in the presence of liquid He^4 as a buffer. We obtained a relaxation time of 140 hours (in a 1 cm diameter cell) that compares with a (crude) theoretically-estimated intrinsic relaxation time of ~ 170 hours.

From these and other data,[12] we conclude (a) the data are presently insufficient to predict with accuracy what the wall-induced relaxation rate (and thus the resultant relaxation time) will be under the conditions proposed for the He^3NG, and (b) a He^4 gas buffer could be used to reduce further wall-induced relaxation if it should be necessary. Unfortunately, unlike the H_2 wall coating, He^4 has a liability as well as an advantage: the addition of He^4 decreases the He^3 diffusion coefficient, and the gradient-induced relaxation rate is increased proportionately.[10] Thus, optimal He^4 density depends on the relative potency of the gradient- and wall-induced relaxation mechanisms. We estimate, however, that with a gradient of 10^{-8} G cm^{-1}, the optimal He^4 density will lead to a relaxation time in excess of 10^5 sec but probably not more than 10^6 sec.

2. Readout Resolution

Since the desired information is encoded at a non-zero frequency, $\nu_o = \omega_o/2\pi$, we can estimate the readout resolution in the limit of a large signal-to-noise ratio with

$$\sigma_\phi \simeq [S_B(\nu_o)/\Delta t]^{\frac{1}{2}} B_{mo}^{-1} \qquad [7]$$

where Δt is the measurement time, B_{mo} is magnitude of the internal magnetic flux density: $\vec{B}_{mo} = (8\pi/3)\vec{M}$, and $S_B(\nu_o)$ is the one-sided magnetometer noise spectral density referred to B_{mo}. This expression is based on the assumption that $\nu_o\Delta t >> 1$. The necessity for this assumption derives

from the fact that this device is blind to small rotations when the instantaneous orientation of the magnetization is orthogonal to the pickup coil. This assumption is unnecessary and the expression in [7] is reduced by a factor of $\sqrt{2}$ if two orthogonal pickup coils and SQUIDs are utilized instead of one. If this were the case (as it undoubtedly would be for a practical instrument), the only bandwidth limitation would be that imposed by the SQUID electronics.

If we assume that the pickup coil consists of a compact filamentary loop in the y-z plane, then $S_B^{\frac{1}{2}}$ is given by[4]

$$S_B^{\frac{1}{2}} = (2/\pi)(2E_n\kappa)^{\frac{1}{2}}a^{3/2}R_o^{-3} ,$$

where $E_n(\nu)$ is the magnetometer energy sensitivity at frequency ν, a is the pickup coil radius, R_o is the sample cell radius, and κ is a slowly varying factor relating the coil cross section to its inductance. The CGK data show that E_n is approximately white and equal to 7×10^{-30} J Hz^{-1} at ν_o and we estimate $S_B^{\frac{1}{2}} \approx 3 \times 10^{-11}$ G $Hz^{-\frac{1}{2}}$. Thus $\sigma_\phi \approx 10^{-5}(\Delta t)^{-\frac{1}{2}}$, if $B_{mo} \approx 3 \times 10^{-6}$ G. As the magnetization decays with the relaxation time T_2, the readout resolution will also deteriorate.

3. Stability of the Larmor Frequency

The most important sources of variation in the Larmor frequency are likely to be (a) variations in $\vec{B}_o$ due to mechanical motion arising from external perturbations or dimensional or penetration-depth variation arising from thermal fluctuations, (b) the varying magnetic field generated in the pickup loop because of noise currents injected into the input circuit by the magnetometer, (c) interaction of the sample magnetization with itself because of asymmetries in the sample cell, superconducting parts (including the shield) and because of finite magnetometer loop gain, and (d) the London moment. It is easiest to consider these effects separately.

a. *Effect of Dimensional and Temperature Stability on* ω_o

Although a detailed design of the gyro case, field coils, etc. is needed to estimate the magnitude of dimensional variations and their effect on the Larmor frequency, we can make some brief remarks. First, because the magnetic field gradient must be small because of relaxation considerations, the effect of small displacements of the sample cell with respect to the spherical shield will be minor. For instance, with a gradient of 10^{-8} G cm^{-1}, a relative displacement as large as 0.1 μm would produce a frequency shift of only $\delta\omega_o \simeq 2 \times 10^{-9}$ rad sec^{-1}. Secondly, the linear expansion coefficient of fused silica at 4.2 K is $\alpha \simeq -3 \times 10^{-8}$ K^{-1}.[13] Now if the field coils were to consist of a persistent superconducting circuit that is deposited on a quartz surface, then $\delta B_o/B_o = \delta\omega_o/\omega_o = -2\alpha\delta T \simeq 6 \times 10^{-8}(\delta T)$, where δT is in degrees Kelvin.

There is an additional effect that can cause B_o to vary as a function of temperature: the penetration depth (i.e., the average depth that a magnetic field penetrates the surface of a superconductor) has a weak temperature dependence for temperatures $T << T_c$, T_c being the transition temperature of the superconductor. This situation is most simply modeled by considering the average magnetic field produced by a persistent current in a superconducting ring that is thick compared to the penetration depth. The model then takes the effective inner radius to be equal to the inner radius of the ring plus the penetration depth. Since the flux through the ring is conserved we have

$$\frac{\delta B_o}{B_o} = -\frac{2\delta r}{r} = -\frac{2}{r}\left(\frac{d\lambda}{dT}\right)\delta T \ ,$$

where r is the inner radius of the ring, and $\lambda = \lambda(T)$ is the temperature-

dependent penetration depth, which for our purposes is given with sufficient accuracy by [14]

$$\lambda(T) = \lambda_o[1 - (T/T_c)^4]^{-\frac{1}{2}} .$$

In the limit that $T << T_c$,

$$\frac{\delta B_o}{B_o} \simeq - \frac{4\lambda_o}{r} \left(\frac{T}{T_c}\right)^4 \left(\frac{\delta T}{T}\right).$$

If the shield is made out of niobium, $T_c = 9.46$ K, and $\lambda_o = 4.7 \times 10^{-6}$ cm.[15] Taking r = 6 cm we then estimate

$$\delta B_o/B_o \simeq - 3 \times 10^{-8}(\delta T)$$

for T = 4.2 K. This is of the opposite sign and approximately one-half the size of the effect due to the coefficient of expansion of the quartz. Temperature regulation at the level of ± 10 mK will therefore lead to variations in ω_o on the order of 3×10^{-10} rad sec^{-1}.

b. *Effect of Magnetometer Noise and Drift on* ω_o

As we have noted previously, it is advantageous to include the superconducting coupling circuit as an element in the magnetometer feedback loop in order to reduce reaction currents. In doing this, the noise currents injected in the coupling circuit by magnetometer noise and drift become accurately known (in the limit of large loop gain) and we can readily estimate their effect from published magnetometer data.

Since the normal to the plane of the pickup loop should be orthogonal to $\vec{B}_o$, the magnetic field generated by small currents in the pickup loop should ideally have only a second order effect on $|\vec{B}_o|$. Because of construction tolerances and because of the ambient field trapped in the shield,

however, the unit normal of the pickup loop will have a small component in the direction of $\vec{B}_o$ of the order of 10^{-3}. This will be much more important than the second order effect.

An analysis based on the CGK data indicates that the effect of linear magnetometer drift becomes dominant over that of random noise after about an hour or so. If we now use the average drift rate over a 20 hour period reported by CGK,[16] we estimate that the Larmor frequency will have changed by $\sim 7 \times 10^{-10}$ rad sec^{-1} after 20 hours. This means that the average gyro drift rate over a 20 hour period will be $\sim 4 \times 10^{-10}$ rad sec^{-1}.

It should be pointed out that the true gyro error is significantly less than this. Because the signal phase is the integral of the Larmor frequency, only low frequency noise components and drift introduce significant error. Since the magnetometer loop gain is quite large at low frequencies ($\sim 10^5$), it should be possible to determine accurately the relationship between ω_o and the low frequency noise and drift that is seen at the magnetometer output. Once this is done, errors introduced by this source can be reduced even further.

c. *Effect of Gyro Housing Asymmetries on* ω_o

It can be shown that the effect of asymmetries in the sample cell and in superconducting components causes a frequency shift that is proportional to $\gamma M_z = \gamma|\vec{M}|\cos\theta$. The fact that the magnetometer loop gain is finite has a similar effect. This leads to a slow variation in ω_o since M_z decays with a time constant T_1. As an example of this type of effect we will write down the appropriate expression for the effect of sample cell asymmetry. It is estimated that other contributions will be of the same order or smaller.

If the radius of the sample cell is expressed in the form

$$R(\theta,\phi) = R_o[1 + \sum_{\substack{\ell m \\ \ell \neq 0}} \beta_{\ell m} Y_{\ell m}(\theta,\phi)] \ ,$$

where $|\beta_{\ell m}| << 1$, $\beta_{\ell -m} = (-1)^m \beta^*_{\ell m}$, and $Y_{\ell m}(\theta,\phi)$ are spherical harmonics (the polar axis being in the direction of $\vec{B}_o$), then it can be shown that only β_{20} has an effect in first order. By defining

$$\delta R_{20} = R_o \beta_{20} Y_{20}(\theta=0) = \sqrt{5/4\pi}\ R_o \beta_{20}$$

the frequency shift due to sample cell asymmetry is simply[4]

$$\delta\omega_{oa} = - (9/10)(\delta R_{20}/R_o)\gamma B_{mo}\cos\theta \ . \qquad [8]$$

In order to evaluate the gyro drift from this source it is necessary to know $\cos\theta$ and its evolution in time. It is reasonable to assume that $|\cos\theta_o| < 10^{-3}$ when the gyro is initialized.[17] There are, however, three mechanisms which can cause the magnetization to move away from the x-y plane: (a) radiation damping due to the magnetometer gain being finite and having a non-zero phase shift, (b) the component of the magnetic-noise field at frequency $\omega_o/2\pi$ that originates from the magnetometer feedback, and (c) the component of random angular displacements of the gyro case about the x and y axes at frequency $\omega_o/2\pi$. The first of these mechanisms will cause $(\theta - \pi/2)$ to vary linearly in time, whereas the latter two will cause θ to execute a random walk so that the variance of $(\theta - \pi/2)$ will increase linearly in time.

Under the conditions that the magnetometer loop gain magnitude is $\sim 10^5$ with an argument $\lesssim 10^{-2}$ rad at $\omega_o/2\pi$, and the platform angular

noise spectral density is $\leq 10^{-6}$ rad $Hz^{-\frac{1}{2}}$ (also at $\omega_o/2\pi$), then it is estimated that θ will not change more than 10^{-3} rad over a period of 10^6 sec (12 d). Since these conditions are quite reasonable, we will assume that $|\cos\theta| \leq 2 \times 10^{-3}$ in equation [8]. By taking $\delta R_{20} = 0.13$ μm, $R_o \approx 1.9$ cm, $B_{mo} = 3 \times 10^{-6}$ G, we then obtain the estimate $|\delta\omega_{oa}| \leq 10^{-9}$ rad sec^{-1}.

d. *Effect of the London Moment*

If a spherical superconductor such as the shield for the He^3NG is rotated with an angular velocity $\vec{\Omega}$, then a uniform field will appear in the interior according to the expression derived by London:[18]

$$\vec{B}_L = \frac{2mc}{e}\vec{\Omega} .$$

Here, m and e refer to the mass and charge of the electron, and the numerical value of the coefficient is 1.14×10^{-7} G rad^{-1} sec. Writing $\delta\omega_{oL} = -\gamma\vec{B}_L$, we have the frequency shift due to the London moment:

$$\delta\omega_{oL} = -\gamma\left(\frac{2mc}{e}\right)\vec{\Omega} = 2.6 \times 10^{-3}\,\vec{\Omega} .$$

Even though this effect is large, it does not represent a true gyro error since it is a well-known systematic effect that can be readily corrected in the data processing.

In order to make use of the estimated stability of the He^3NG, it is necessary that the stability of the clock used to measure the phase of the He^3NG output signal not be a limiting factor. There are, however, a number of clocks that have fractional frequency stability (Allan variance) of 10^{-11} or better for sampling times in excess of 1 sec.[19] Thus there should not be any problem in principle, but care will be needed in making

the phase measurement if the intrinsic stability of both the clock and the He^3 NG are to be successfully utilized.

III. Work during Contract Period

1. New Low Field Facility

One of the most important aspects of the cryogenic He^3NG is the ultra-low field facility. Over the past number of years we have developed considerable experience in techniques for cooling superconducting shields such that there is very little flux trapped in the shield. Recently, however, we have devised an improved technique using a new cooling apparatus. During this past period, this technique has been experimentally tested. This new process is designed to significantly reduce thermal gradients which can produce excess trapped field during the cooling process. As a result of this development, we have successfully produced an 8" diameter shield for the He^3 nuclear gyro which has a field level of 2×10^{-8} gauss over a substantial volume (Fig. 3). This surpasses our target of 5×10^{-8} gauss and to the best of our knowledge is the lowest absolute magnetic field region ever made.

2. Precision Gyro Housing and Cryostat Probe

During this period the precision ground fused silica components of the new gyro housing were received at Stanford (Fig. 4). The sample cell can now be tumble lapped to within 5 microinches of sphericity and assembled by optical contacting. The only additional work that might precede final assembly of the housing components is the deposition of the superconducting shield material on the inner hemispherical surfaces of the outer shell. This step, however, can (and probably will) be delayed until after initial tests have been made on the precision gyro assembly.

In addition to the gyro housing, a cryostat probe that will be used for testing pruposes is under construction along with an airlock assembly. The airlock assembly allows the cryostat probe to be slowly lowered into the dewar containing the low field so as to minimize thermal shock of the gyro components and minimize boiloff of liquid helium.

Fig. 3

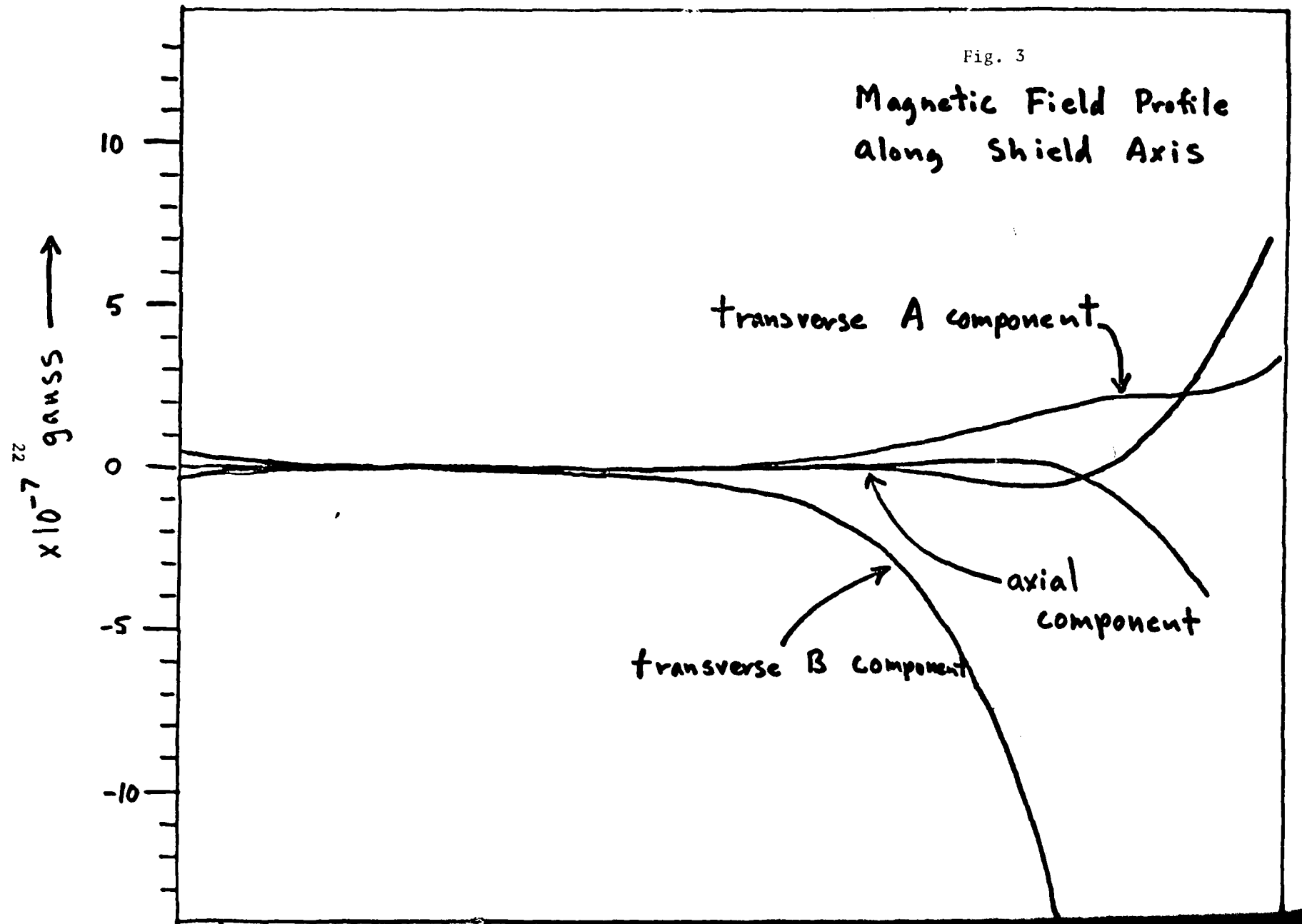
Magnetic Field Profile
along Shield Axis
10
5
0
-5
-10
$\times 10^{-7}$ gauss
transverse A component
axial
component
transverse B component

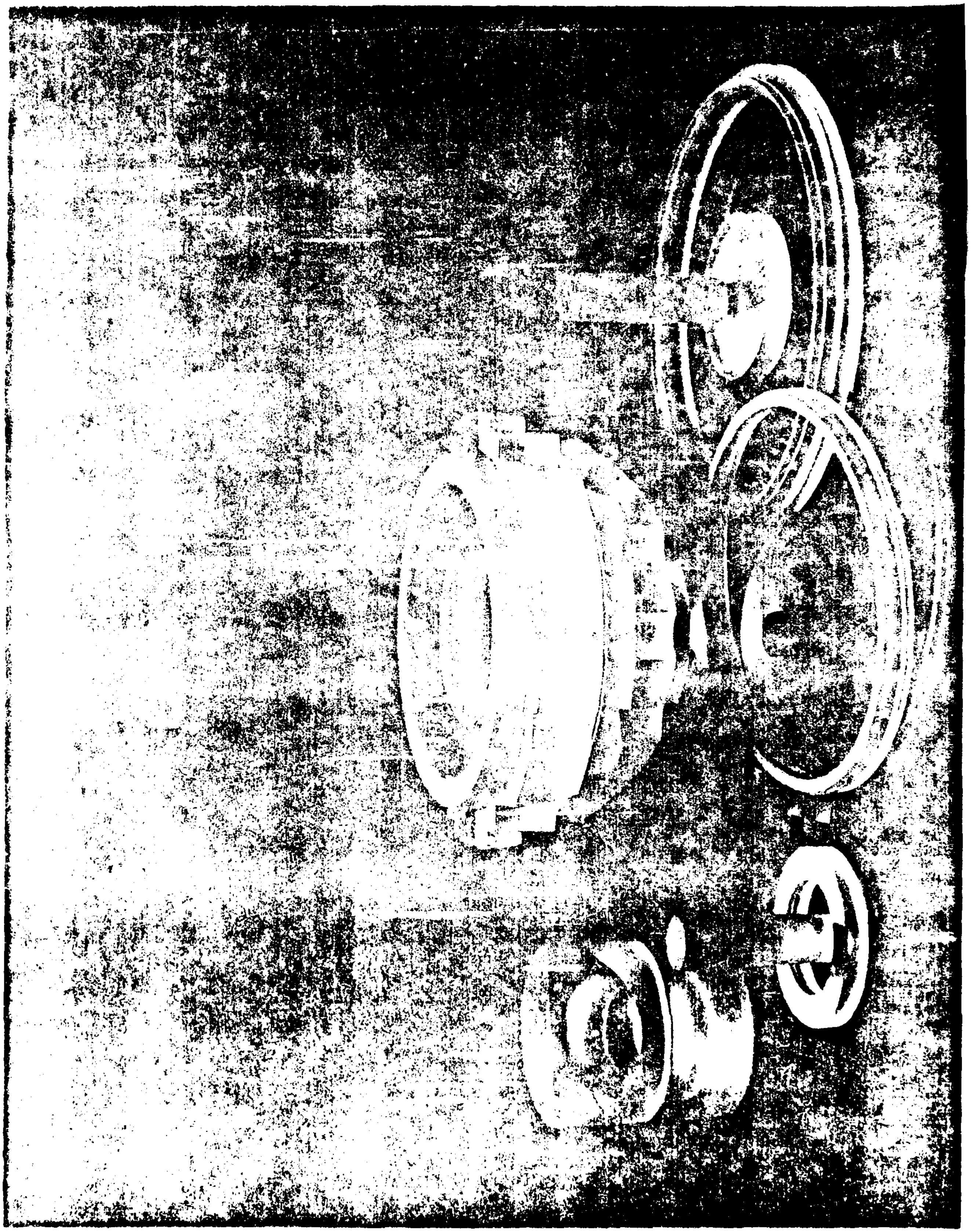

Fig. 4. Precision-ground fused-silica components to be assembled for the new gyro housing.

3. Engineering Analysis of the Cryogenic He^3NG

During this period a final copy of the engineering Ph.D. thesis of Capt. G. Shaw was submitted to the department of aeronautics and astronautics. This work investigated kinematic rectification in nuclear gyros (the response to small-angle coning of the gyro case about the input axis), the mechanism of cross-coupling (i.e., how to reduce the error introduced by the rotation of the case about an axis orthogonal to the input axis), and gyro drifts induced by acceleration or thermal gradients in the presence of a magnetic field gradient. A practical compensation technique for the coning effect has been devised. These effects can occur in any kind of nuclear gyro. Copies of the thesis are being included as a part of this report. In addition to the analysis, an experimental technique to check the results of the kinematic rectification effect was devised. This technique involves applying a circularly polarized magnetic field transverse to the input axis in order to simulate the coning of the gyro case.

IV. Experimental Results Obtained from the Improvement of the Old Apparatus

1. Modification of Apparatus

Analysis of the data obtained from our original apparatus suggested that the T_1 measurements and possibly the free precession decay measurements were strongly affected by a dipolar magnetic field gradient arising from a contaminant speck located near the sample cell (see Figures 5 and 6). Moreover, strong circumstantial evidence indicated that this contaminant dipole moment was located in the plastic pick-up coil form. Since this part of the apparatus could be readily modified, it was thought worthwhile to replace all the plastic components near the sample cell with Macor parts. (Macor is a machinable glass-ceramic which has been found to be magnetically very clean.) The Macor field-coil assembly incorporated yet another improvement over the plastic assembly in that it had three orthogonal field coils instead of the previous two.

There were several motivations behind making these improvements in the original apparatus. First, it was hoped that the remaining apparatus would be sufficiently clean to allow it to be operated as a crude nuclear gyro. Secondly, if this turned out to be the case, to use it to test a number of model predictions obtained in our theoretical analyses. And finally, to try to use it as a probe of our new ultra-low field shield. As will be discussed in the next subsection, it was found that the use of the field coil assembly did substantially reduce the contaminant-dipole problem. This improvement made it possible to undertake a more extended and systematic study of free-precession decay characteristics than had been previously possible. As a result of this study it was found, however, that the self-induced field gradient arising from the interaction of the sample magnetization with the third surface harmonic of the sample cell was much larger than had been previously suspected. The details and implications of this discovery will be discussed in subsection c.

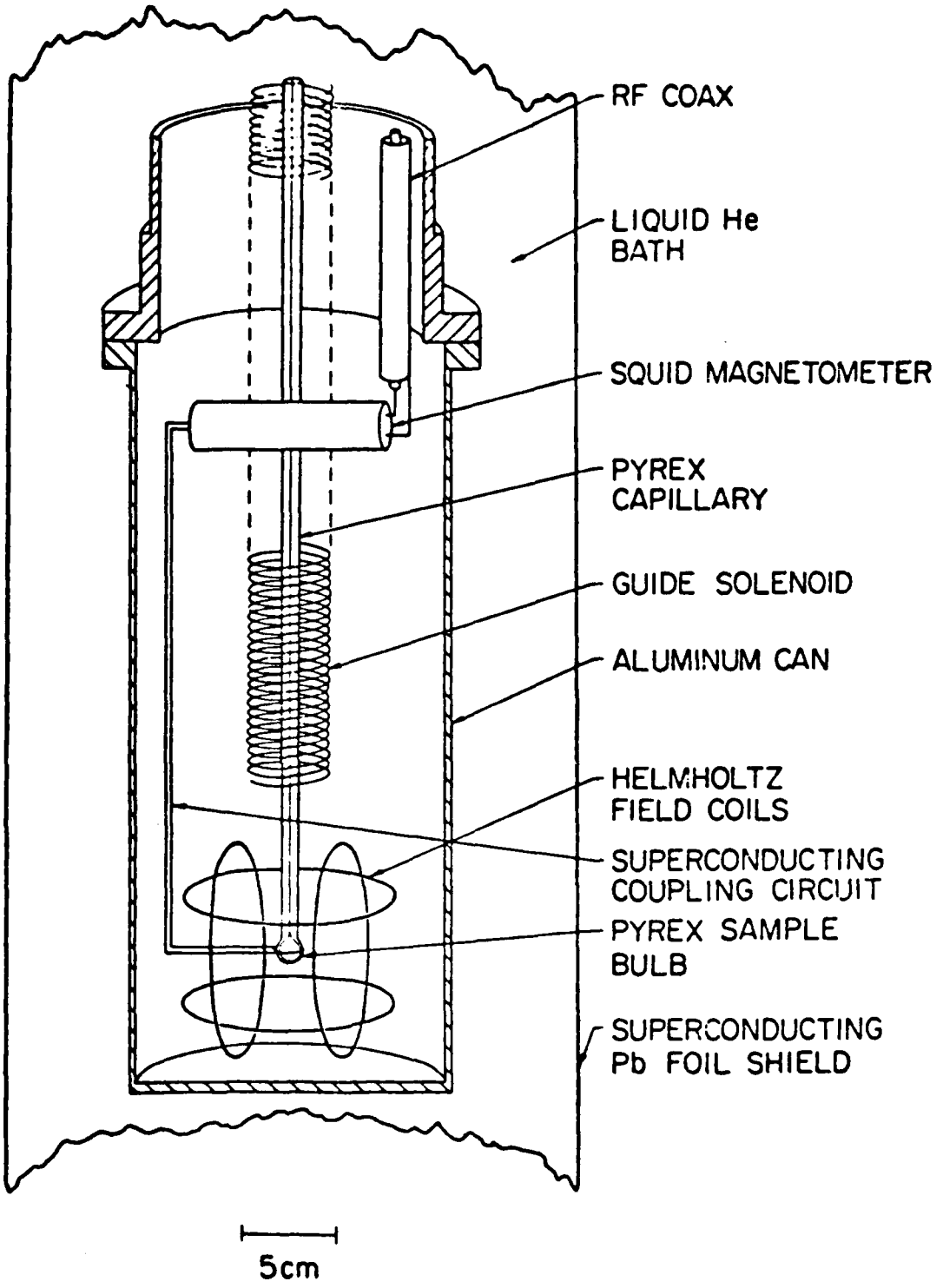

Fig. 5

Schematic depiction of the bottom portion of the cryostat probe.

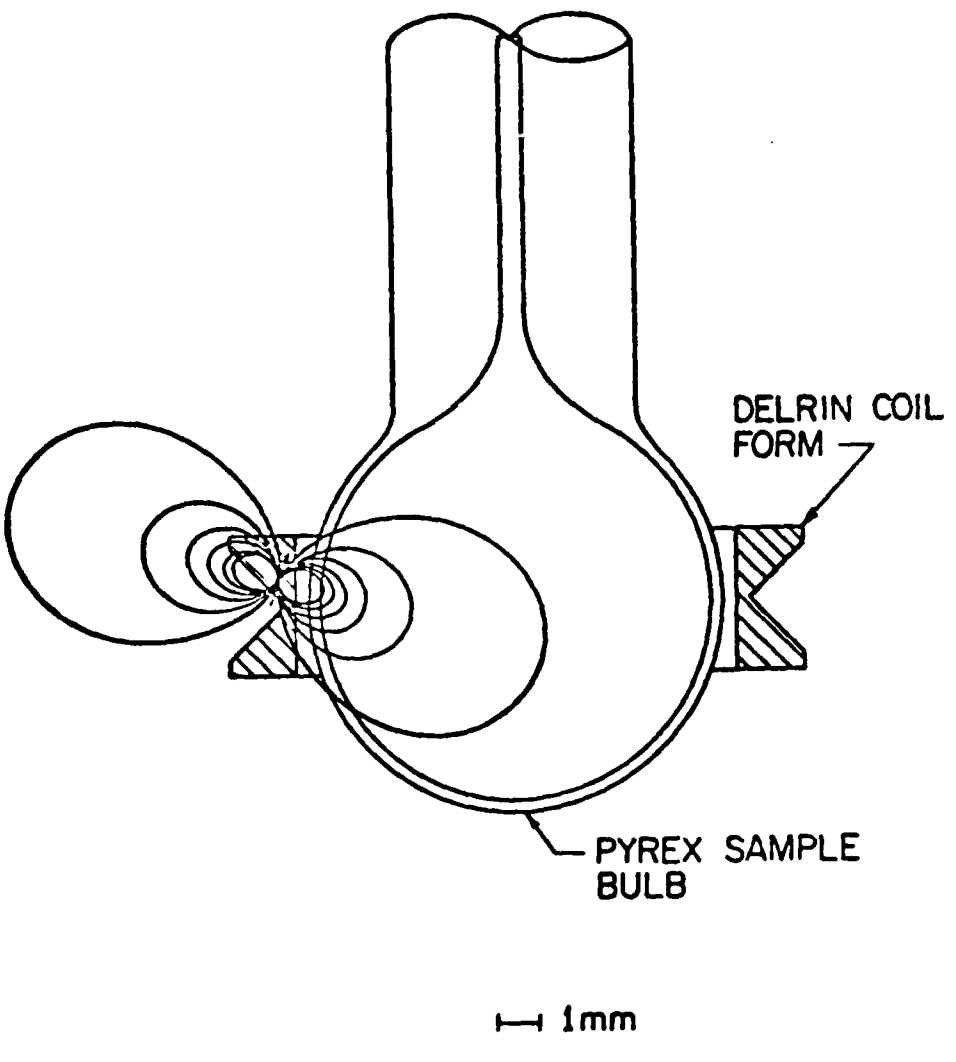

Fig. 6

Detail of sample cell and pickup coil form showing possible location of a ferromagnetic dipole.

2. T_1 Measurements on Liquid Mixtures Obtained from the Modified Apparatus

A sequence of longitudinal relaxation time (T_1) measurements were made on a standard He^3-He^4 liquid mixture (He^3 concentration of 7×10^{-4}) as a function of the applied uniform field, B_o, as a diagnostic check of the modified apparatus. The results of these measurements are plotted in Fig. 7 as T_1^{-1} vs. $B_o^{-3/2}$. It can be shown that the longitudinal relaxation rate of a sample exposed to a dipolar perturbation arising from a macroscopic moment located at a distance from the sample cell that is small compared to the cell diameter is of the form $T_1^{-1} = T_{1\infty}^{-1} + \alpha B_o^{-3/2}$, where

$$\alpha \simeq 3\pi m^2 (\gamma D)^{\frac{1}{2}} / (4\sqrt{2}\, V b^4).$$

In this expression, V is the sample cell colume, D is the He^3 diffusion coefficient, m is the magnitude of the contaminant dipole moment, γ is the He^3 gyromagnetic ratio, and b is the distance between the dipole and the nearest boundary of the sample cell. In order for this expression to be valid it is necessary that $|\vec{B}_o| >> |\vec{B}_1|$ everywhere in the sample cell ($\vec{B}_1$ is the perturbation field arising from the contaminant dipole), and $B_o >> D/\gamma b^2$.

If the lowest two field points (taken at 4.3 and 14 G) are omitted and the data replotted on a larger scale (Fig. 8) it is seen that that data fits the $B_o^{-3/2}$ dependence quite well for $B_o \geq 42$ μG. A least squares fit to this data yields an estimate for the parameter $\alpha \simeq 3.80 \times 10^{-12}$ sec^{-1} $G^{3/2}$. This is a factor of five smaller than the value obtained with the Delrin coil forms which is also shown in Fig. 8 for comparison.

From this T_1 data we can draw the following conclusions: 1) The dominant dipolar perturbation field that was noted in our original data was indeed due to magnetic contaminant in the Delrin plastic coil forms. 2) The replacement of the plastic coil forms has resulted in a factor of five improvement in the magnetic-gradient induced relaxation due to nearby dipole moments. 3) One or both of the validity requirements for the $B_o^{-3/2}$ dependence are violated in

Fig. 7. Longitudinal relaxation rates as a function of the applied field over a range of 14.2 microgauss to 1.4 milligauss.

Fig. 8. Same data as in Fig. 7 plotted on a different scale. Lower curve are the data taken with Macor coil assembly and the upper curve is a typical least-squares fi* obtained with the original plastic coil assembly.

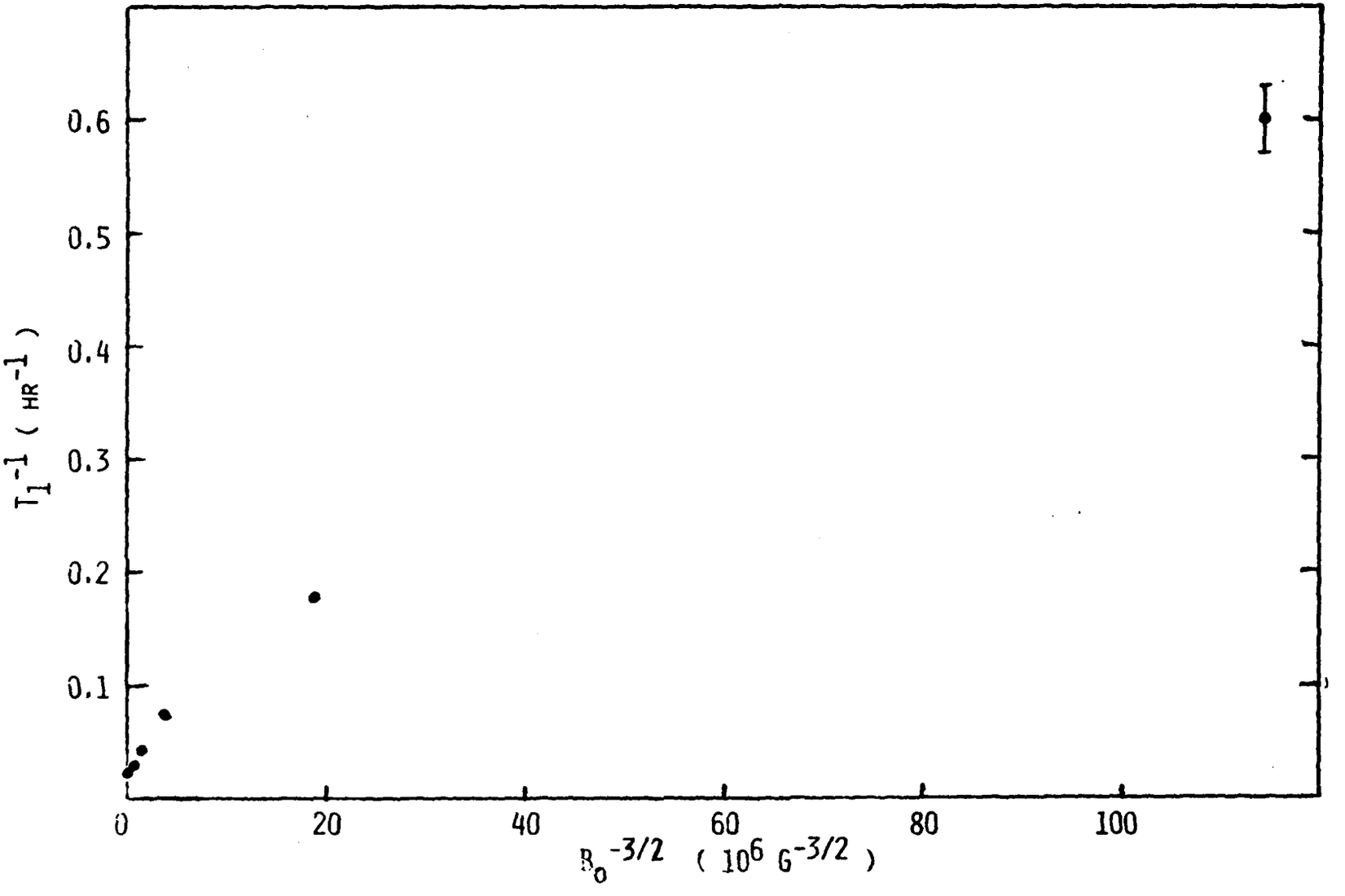

Fig. 7

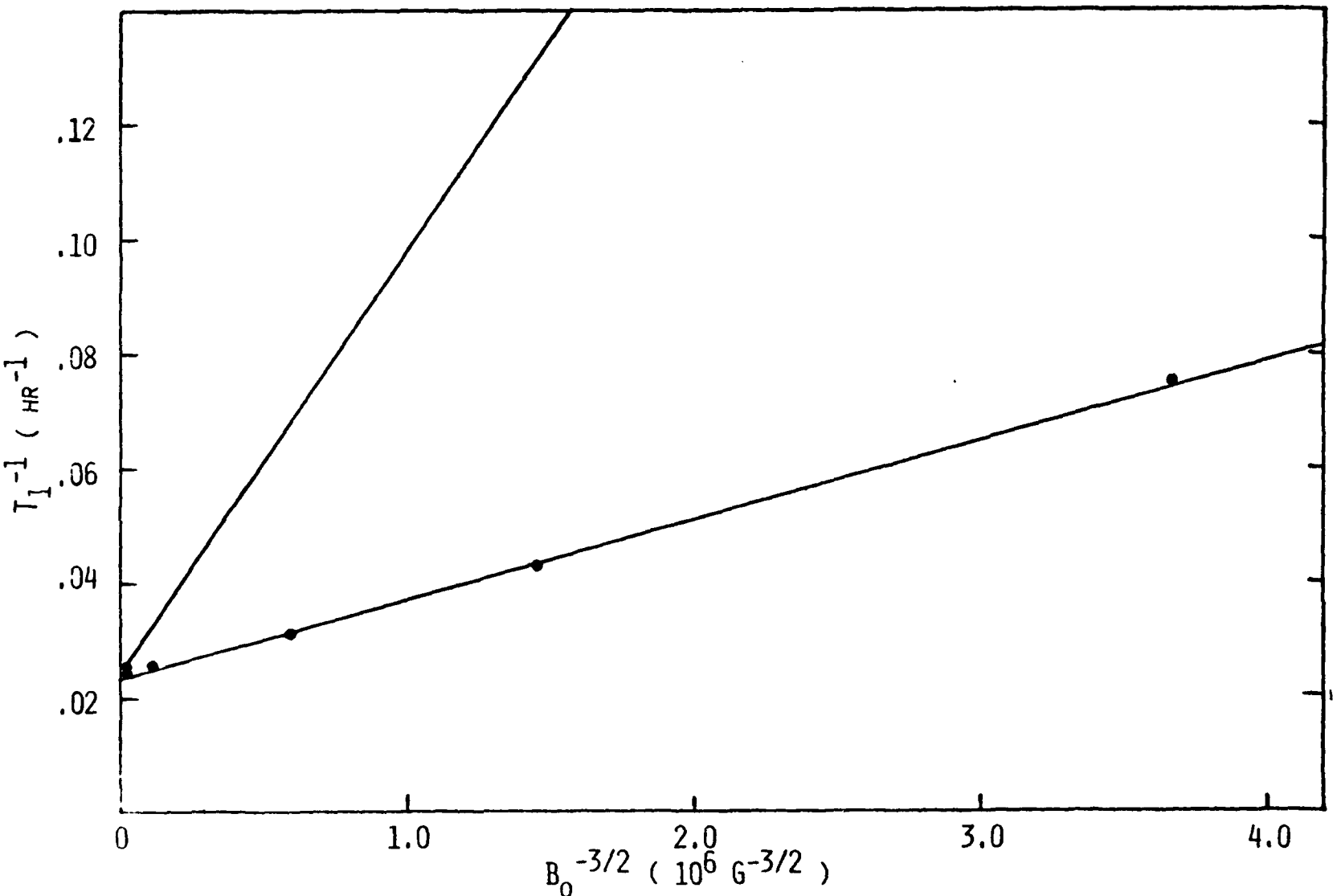

Fig. 8

fields less than 40 μG. This last conclusion in conjunction with the measured value of the slope parameter, α, leads us to suspect that the residual dipole moment that is still observed is located either in or on the Pyrex wall of the sample cell itself. This suspicion has no direct implication for the new precision gyro housing since the new sample cell is much larger and is made of high purity fused silica fabricated by precision grinding and lapping rather than glassblowing. This result, however, does point out the importance of using a non-magnetic lapping compound (aluminum oxide rather than rouge or cerium oxide) and rigorous cleaning procedures.

3. Free Precession Decay Measurement

a. Introduction

Of more direct importance to the gyro applications than the longitudinal relaxation time is the decay of the transverse component of the magnetization during free precession. It is essential that long transverse decay times be obtained in order that precision rotation-rate measurements can be made. In what follows we will first discuss the general aspects of free precision decay analysis and the kind of information we hoped to obtain from this type of measurement. Experimental results obtained from our modified apparatus will then be discussed in the light of two different kinds of analysis. These new results represent a significant improvement over our previous measurements in that they include some transverse decay times that are an order of magnitude longer than any we had previously obtained.

As is discussed in detail in the thesis of M. A. Taber, there are two limiting physical circumstances where free precession decay (fpd) data are readily analyzed. These two cases are separated by the motional narrowing boundary $\gamma^2 B_1^2 \tau_c^2 \sim 1$, where $\vec{B}_1$ is the perturbation field responsible for transverse decay and τ_c is the correlation time associated with the perturbation.

The perturbation field is a random variable in time because of the diffusive motion of a given nuclear spin throughout the sample cell and is defined to have a zero mean. $\vec{B}_1$ can be either microscopic or macroscopic in origin. In the former case, the perturbation field arises from a nearby nuclear or electronic spin, and in a rough sense τ_c is on the order of the time necessary to diffuse an atomic diameter. In the latter case, $\vec{B}_1$ is the inhomogeneous component of the macroscopic field and τ_c is roughly the time necessary for an atom to diffuse from one side of the sample cell to the other. In our situation, the effect of microscopic interactions on the transverse decay is quite weak compared to that of macroscopic field gradient, and the current discussion deals exclusively with the macroscopic case.

When the motional narrowing condition $\gamma^2 B_1^2 \tau_c^2 \ll 1$ is well satisfied, motion of the individual He^3 atoms is sufficiently rapid with respect to the rate that the perturbation field can reorient a nuclear spin that the perturbation field is largely averaged out and has only a second order effect. In this limit the sample magnetization is uniform throughout the sample and the transverse decay can be analyzed by standard density matrix (Redfield) spin relaxation theory. The theory yields a time dependence of the transverse component of the magnetization of the form $\exp(-t/T_{2G})$. The motionally-narrowed limit represents the most desirable circumstance with regard to nuclear gyro applications in that the only effect that the perturbation (gradient) field has on the Larmor frequency is a second order frequency shift that is constant in time if the gradient itself is time-independent.[4]

If the motional narrowing condition is strongly violated, the fpd has a significantly different character. In this case the diffusion is relatively slow and the spins process with a Larmor frequency given by the local field magnitude. The sample magnetization then becomes nonuniform. In this limit

the effect of spin diffusion on the fpd is secondary. If it is assumed that all portions of the sample cell are equally coupled to the pickup coil (which is a good approximation with the modified coil assembly) and the gradient field is such that $|\vec{B}_1(\vec{r})| \ll B_o$ everywhere in the sample cell, then the transverse fpd signal represents the Fourier transform of the lineshape function. The lineshape function is an unnormalized distribution function of the z component of $\vec{B}_o + \vec{B}_1(\vec{r})$ over the sample volume where $\vec{B}_o$ is taken to be in the z direction. An fpd arising from this kind of situation is not as useful for nuclear gyro applications as a motionally-narrowed fpd, since any lineshape asymmetry can cause a time-dependent phase shift which would simulate a rotation. In spite of this, however, an fpd obtained from a situation where the motional narrowing criterion is strongly violated does not represent useless information, since it can be readily analyzed to provide useful diagnostic information; i.e., the field distribution function.

Because of the importance of the motional narrowing criterion, it is useful to make things more concrete by specifying some of the numbers which typify our experimental situation. In the case of a spherical geometry, the slowest diffusion mode has a time constant $\tau_{11} = 0.2308\ R_o^2/D$, where R_o is the radius of the sample cell and D is the He^3 diffusion coefficient. In our case $R_o \simeq 0.5$ cm and $D \simeq 10^{-4}$ cm^2 sec^{-1} for He^3 in liquid He^4. Thus the longest correlation time associated with diffusive motion is $\tau_{11} \simeq 10$ min. If we now consider for the sake of definiteness a uniform gradient of the form $B_1(r) = g(\hat{i}x - \frac{1}{2}\hat{j}y - \frac{1}{2}\hat{k}Z)$, then the motional narrowing criterion becomes $\gamma^2 B_1^2 \tau_{11}^2 = (3/10)R_o^2 g^2 \gamma^2 \tau_{11}^2 \simeq 0.02\ g^2\gamma^2 R_o^6 D^{-2} \ll 1$. For the numbers that have been specified this means that $g \ll 3 \times 10^{-7}$ G cm^{-1}. If it is assumed that the motional narrowing condition is indeed satisfied, then an expression for the transverse

decay time constant T_{2G} can also be obtained for our hypothetical gradient:

$$T_{2G}^{-1} = \tfrac{1}{2}(0.0229)\gamma^2 g^2 R_o^4 D^{-1} ,$$

where it has been very reasonably assumed that $\omega_o \tau_{11} >> 1$. If this expression is combined with the motional narrowing criterion, then it is seen that $T_{2G} >> 6\ \tau_{11}$. Thus the signature of motional narrowing in our experimental environment would be an fpd with an exponential envelope having a time constant of more than one hour.

b. Fourier Analysis of Experimental FPD Data on a Liquid Mixture

Free precession data of a standard He^3-He^4 liquid mixture (He^3 concentration of 7×10^{-4}) were initially taken on a chart recorder but were subsequently taken by analog-to-digital conversion in order to facilitate discrete Fourier analysis by computer. The technique used was to start with the magnetization initially aligned with the applied field, $\vec{B}_o$. The applied field was then adiabatically shifted in direction by an angle equal to the desired precession cone half-angle followed by suddenly restoring $\vec{B}_o$ to its original direction. The magnetization then precessed in a cone about $\vec{B}_o$ until the transverse component decayed to zero. The precession core half-angle was selected to be 45^o since this gave a signal that was 70% of the maximum attainable (with a half-angle of 90^o) but resulted in the loss of only 30% of the magnetization per each fpd measurement. The loss in the longitudinal component of the magnetization was small since the longitudinal relaxation time (T_1) was typically much longer than even the longest fpd measurements. In all the measurements to be discussed here, the value of $|\vec{B}_o|$ during the fpd was selected to be 61.7 μG so that the Larmor frequency was 0.2 Hz.

The digitally recorded data were analyzed using standard discrete Fourier transform (dft) techniques. Because of the one-sided nature of the data record (i.e., no data exists before t = 0), however, some care had to be taken to remove phase shifts and time delays before symmetrizing the data and performing the dft. Data which were obtained from a sequence of fpd measurements made during a single run and were thus analyzed are shown in Figs. 9-15. There are only two parameters which vary between these fpd transforms: the direction of the applied uniform field, B_o, and the magnitude of the magnetization. In the first and second fpd, B_o was in the vertical direction (i.e., the fill line direction), and in all other fpd's, B_o was in the horizontal direction. The magnitude of the magnetization also monotonically declines from one fpd data record to the next because of the loss of the transverse component.

Figs. 9-15. Fourier transforms of free precession decays (lineshape functions) of a liquid mixture as a function of initial $B_{mo} = 8\pi\bar{M}/3$, where $\bar{M}$ is the average sample magnetization. Magnetometer sensing direction is horizontal and is designated the x direction. The z direction is taken to be vertically upward. In all cases, the static field magnitude is $B_o = 61.7$ μG.

Fig. 9. Both $\vec{B}_o$ and $(\vec{B}_{mo})_z$ in +z direction

Fig. 10. $\vec{B}_o$ in -z direction and $(\vec{B}_{mo})_z$ in +z direction

Fig. 11. $\vec{B}_o$ in -y direction and $(\vec{B}_{mo})_y$ in +y direction

Figs. 12-15 $\vec{B}_o$ in +y direction and $(\vec{B}_{mo})_y$ in +y direction

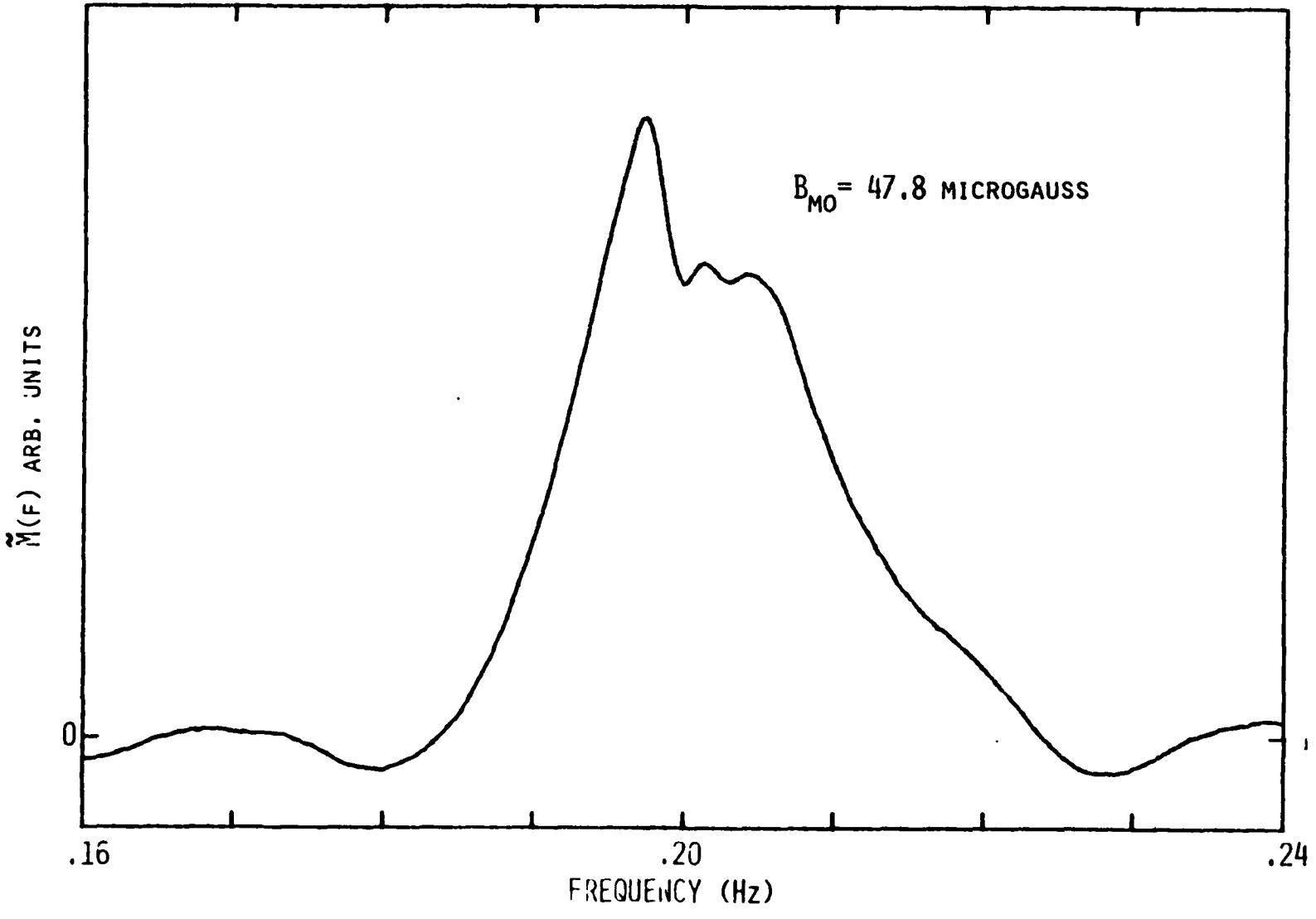

Fig. 9

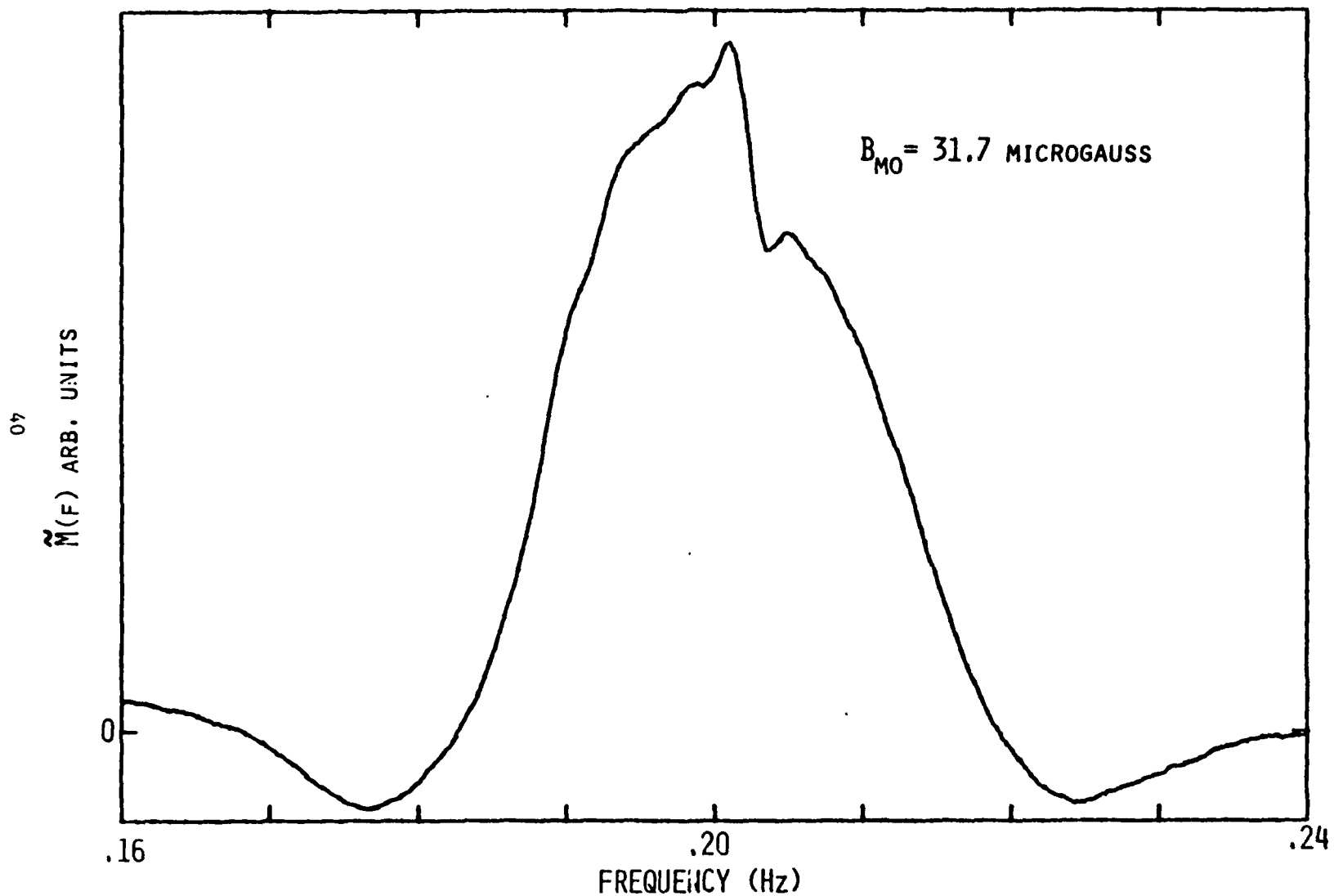

Fig. 10

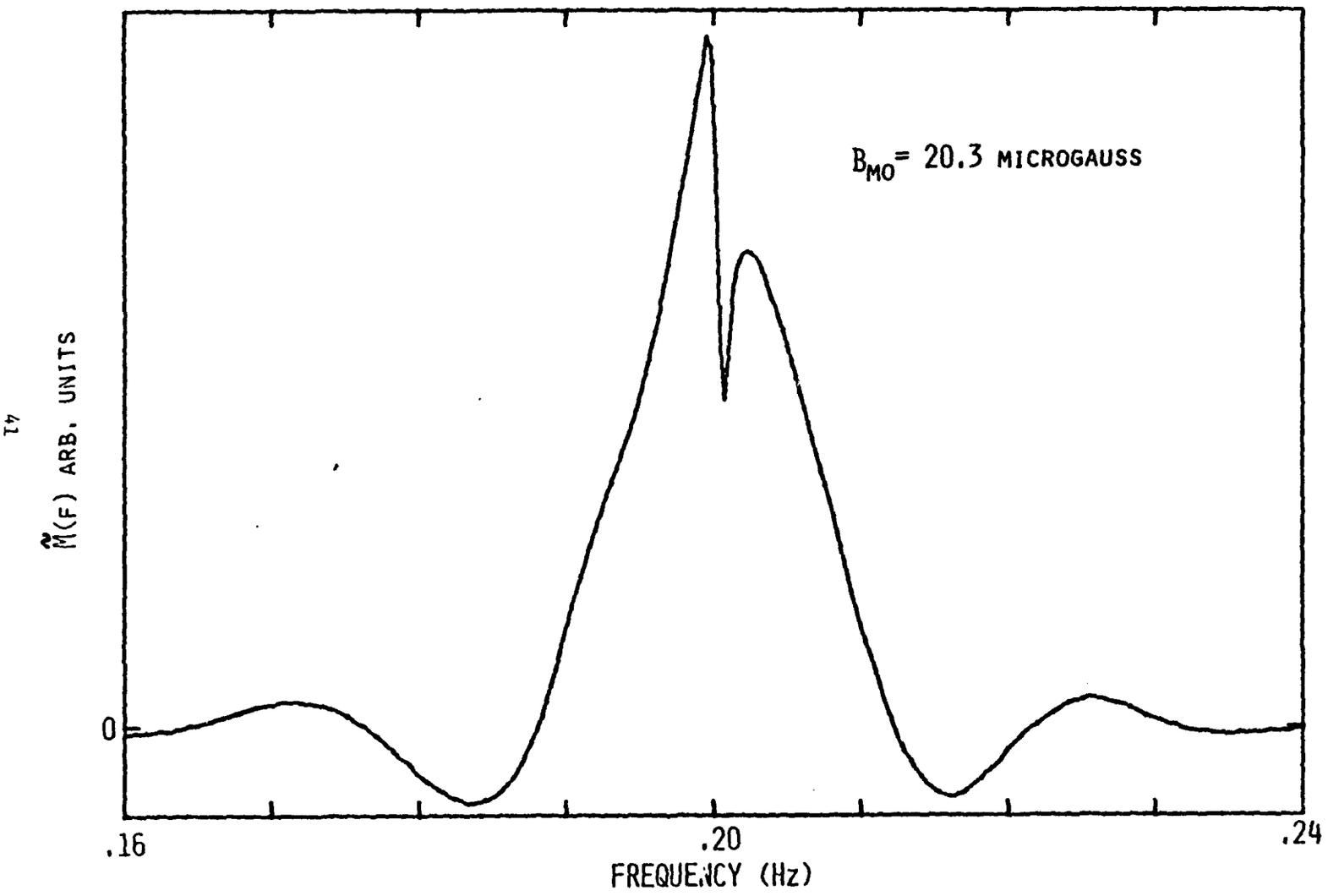

Fig. 11

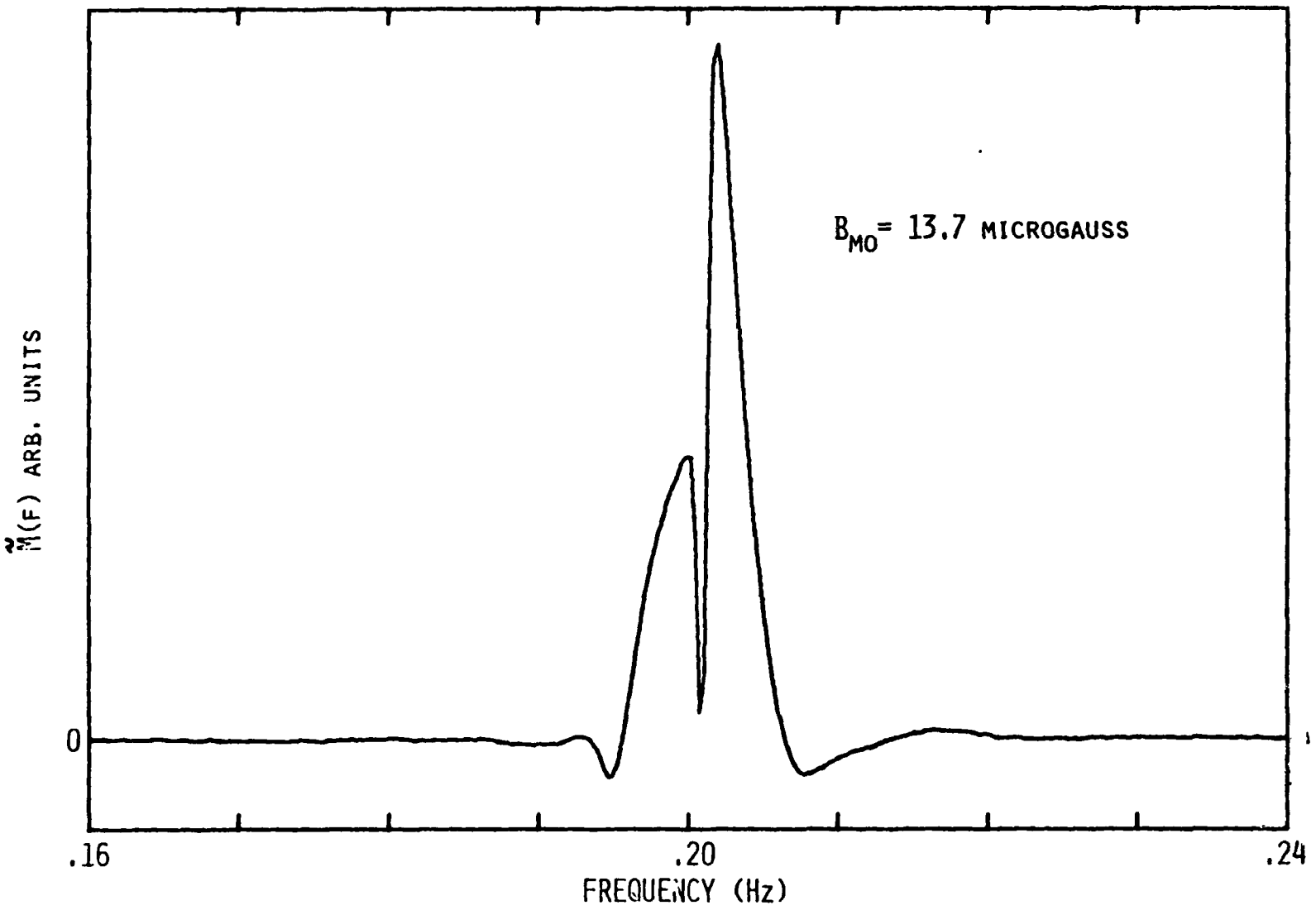

Fig. 12

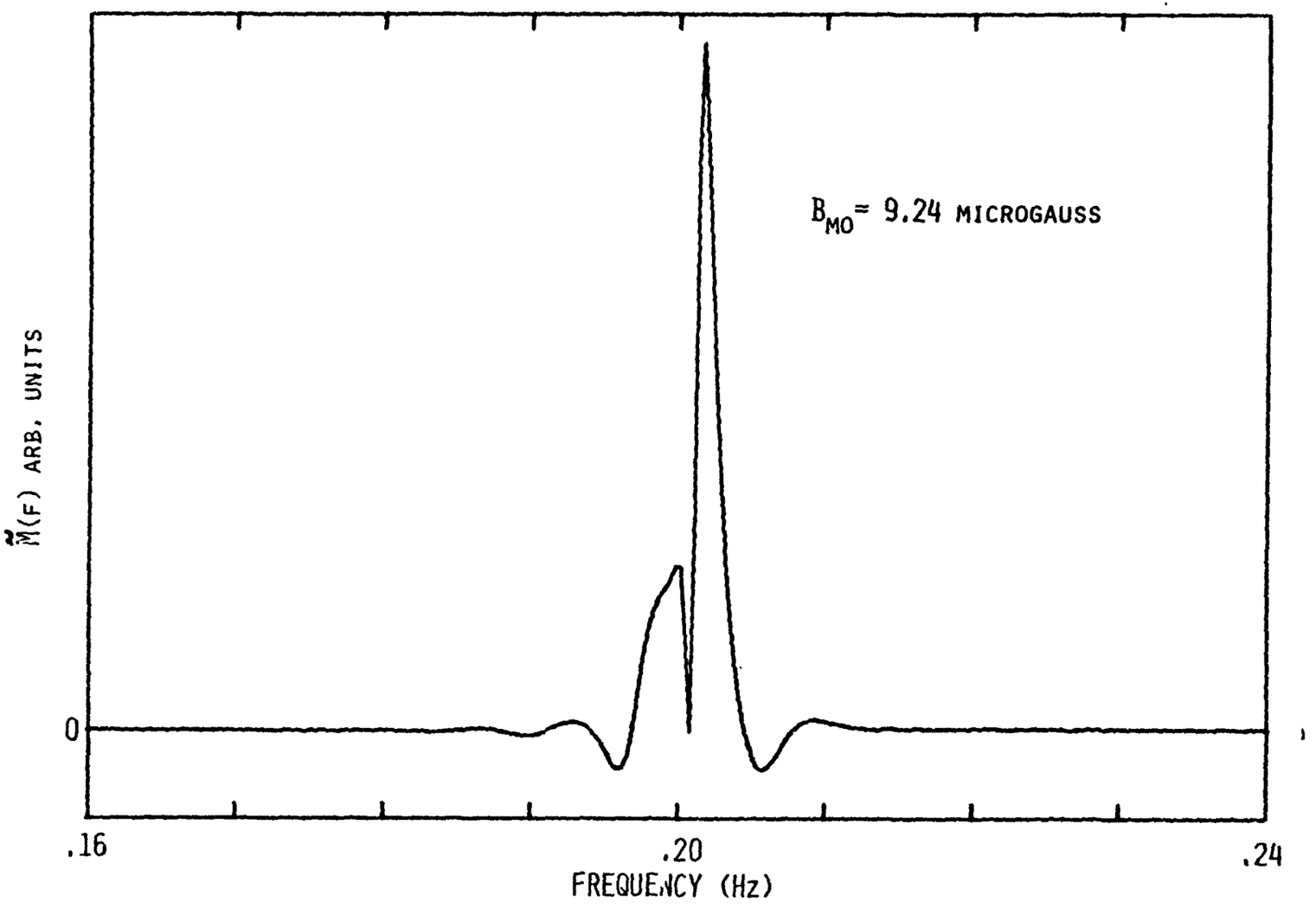

Fig. 13

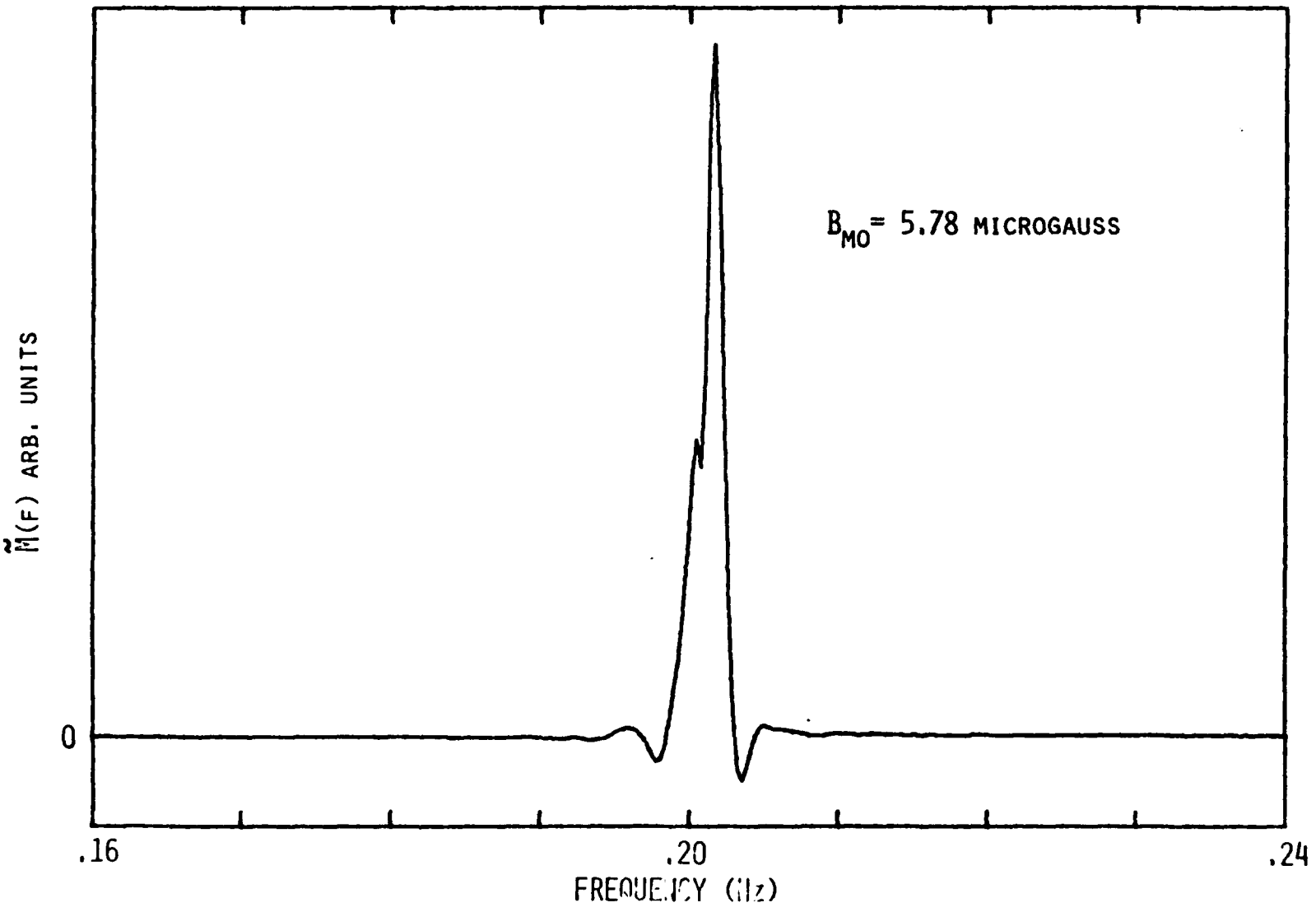

Fig. 14

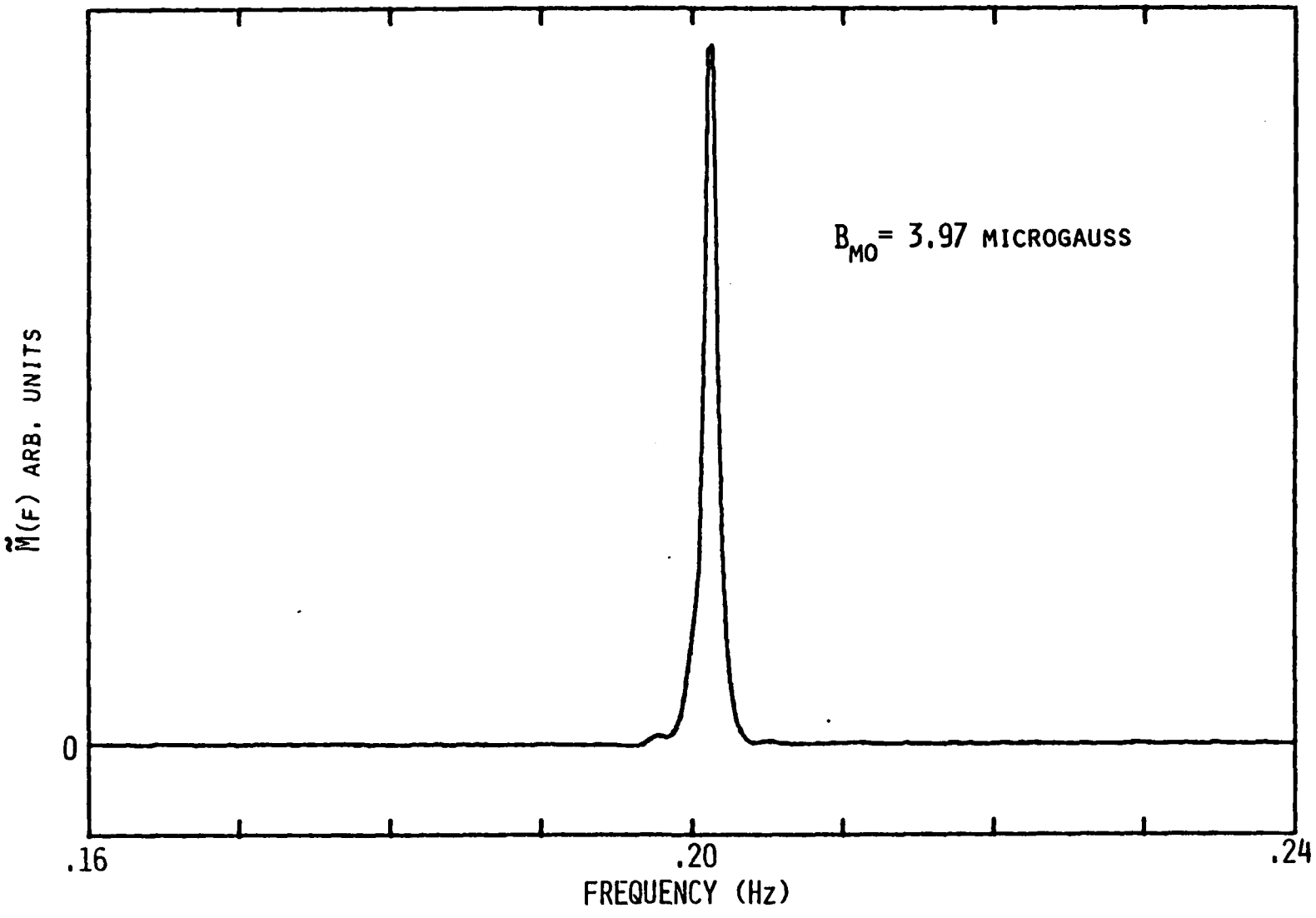

Fig. 15

There are a number of noteworthy aspects of these linshape curves. First, the linewidths decreased markedly as the magnitude of the magnetization decreased. This effect was noted during the fpd data taking and forced longer and longer (up to 40 minutes) data records to be made. Secondly, there are features of the lineshape curves which are physically implausible if they are viewed in a straightforward manner as distribution functions of the z component of $\vec{B}_o + \vec{B}_1(\vec{r})$. In particular, the curves have "wings" where the lineshape function changes signs, and in addition there frequently is a very sharp jump in the middle of the line. It was at first thought that these features were artifacts due to errors in the analysis. Subsequent work, however, made it clear that the analysis was correct but that the simple distribution function model was totally inadequate.

The reason for the inadequacy of the simple model is that the large scale gradient (as opposed to the localized dipolar perturbation which dominates the T_1 data) is dominated by the gradient arising from the sample magnetization due to asphericity of the sample cell shape. In what follows we will describe in somewhat more detail the mechanism for the generation of the gradient. We will then discuss in qualitative terms how a gradient arising from the magnetization itself introduces significant complexities beyond the normal inhomogeneous line broadening that is usually encountered in spin resonance experiments. The problem is sufficiently complex that a more quantitative analysis has not been undertaken since the new precision sample cell will reduce the effect by many orders of magnitude.

c. Self-Induced Broadening Due to Sample-Shape Asphericity

The internal macroscopic $\vec{B}$-field produced by a uniformly magnetized sample is in general not uniform unless the sample shape is ellipsoid, spheroid or a sphere. In most spin resonance experiments this is of little consequence since the sample magnetization is sufficiently small that the gradient thus produced

is trivial compared to the gradient in the applied field. In our case, however, the combination of a large magnetization, very small gradients in the applied field, and the sample shape have conspired to make the opposite true.

In the thesis of M. A. Taber, a calculation is outlined which allows the first-order estimation of the internal magnetic-field structure of a nearly spherical, uniformly magnetized sample. In general this calculation shows that if the deviation of the sample shape from spherical is expanded in spherical harmonics and if the internal magnetic field is specified in terms of a magnetic scalar potential which is likewise expanded in spherical harmonics, then the coefficients of the two expansions can be related to each other in first order by the usual quantum mechanical angular momentum coupling coefficients. The third "angular momentum" turns out to have the value $\ell = 1$. Thus, by using triangle rule and parity consideration one can quickly obtain an intuitive assessment of which sample cell shapes will be important in generating a specified field structure. In our particular case, we are mostly interested in the uniform gradient (Y_{2m}) terms in the field structure. If the coordinate system is chosen such that the coefficients of the Y_{1m} terms in the cell-shape expansion are zero, the only terms that have a first-order effect in producing a uniform gradient are the Y_{3m} terms. Since Y_{30} represents a pear-shape perturbation, it is clear from the shape of our sample cell (Fig. 6) that the Y_{3m} terms are likely to be very important if not totally dominant in the cell-shape expansion. Thus, it is not too surprising that a gradient that is proportional to the sample magnetization has been observed in our apparatus.

The fact that the magnetic field gradient is related to the sample magnetization has a number of significant implications. The most obvious one is that as the magnitude of the sample magnetization decreases, the linewidths would

get narrower as we have experimentally observed. By writing the magnetization as $\vec{M} = \vec{M}_{\parallel} + \vec{M}_{\perp}$, where $\vec{M}_{\parallel}$ is the component of $\vec{M}$ in the direction of $\vec{B}_o$ and $\vec{M}_{\perp}$ is the precessing transverse component, a number of other implications can be perceived. First, as $\vec{M}_{\perp}$ decays during a fpd the the magnitude of the gradient can be expected to decrease and its structure change. Qualitatively one would expect the fpd to show a rather rapid initial dephasing followed by a long "tail" during which the decay is much slower. This type of behavior can explain the presence of the sharp dispersive feature, which arises from the long tail, in the middle of a broader line, which is due to the initial rapid decay. (The fact that the sharp feature is a jump rather than a peak is due to the fact that the phase of the tail is shifted with respect to the initial precession phase.) The presence of the negative wings, however, remains obscure.

Another implication of the self-induced broadening model is with regard to the spatial uniformity of the transverse component of the magnetization. Initially the magnetization would start out fairly uniform, but as the precession proceeds, dephasing will cause significant inhomogeneities in $\vec{M}_{\perp}$ to arise. At this point, of course, it is no longer possible to simply estimate the internal macroscopic field structure. The presence of spin diffusion, however, tends to reduce the spatial variation of $\vec{M}_{\perp}$, and at the same time causes the dephasing to be irreversible. If $M_{\parallel}$ is not too large (or is optimally oriented with respect to the sample cell shape) and the average of $\vec{M}_{\perp}$ becomes sufficiently small, it <u>may</u> become possible for the internal field gradient to be small enough to approach the motional narrowing condition. In this case, the magnetization would once again become fairly uniform and the tail of the fpd would be exponential with a long delay time with respect to the diffusion time. Because our data in some of the latter field measurements had an appearance that suggested that the motional narrowing condition was at least being approached, a separate

type of analysis was carried out to investigate this possibility.

d. Envelope Analysis of FPD Tails

The raw data from the last four fpd's where the initial magnitude of the internal B-field due to the sample magnetization ranged between 14 and 4 μG was subjected to a digital detection and filtration routine which yielded the amplitude (envelope) of the fpd signal as a function of time. The logarithm of the amplitude was then plotted and inspected for linear behavior in the latter portion of the record. In three of the four records which were examined this way it was found that the amplitude of fpd tail did indeed decay exponentially. In one exceptional case the onset of the exponential tail was anomalously delayed, and since the sequence of events prior to recording this particular fpd was significantly different from the others, this particular record was omitted from further analysis. The remaining three, however, were subjected to a least squares fit to an exponential decay. An example of one of the fits is shown in Fig. 16 and in Fig. 17 the value of the three transverse decay rates (T_2^{-1}) thus obtained are plotted as a function of the magnitude of the initial average internal B-field due to the sample magnetization ($B_{mo} = 8\pi M/3$).

Fig. 17 indicates that the transverse decay rate is a monotonic function of B_{mo}. This is presumably due to the self-induced gradient still being a significant contributor to the relaxation rate. The longest T_2 was 21 minutes, which was obtained for $B_{mo} = 4$ μG. Since the slowest diffusion mode decay time is approximately 10 minutes, it appears that this represents being on the border of motional narrowing. It will be recalled that it would be necessary for T_2 to be in excess of an hour in order for motional narrowing to be clearly established. Another indication of the marginal nature of the situation is the fact that one data record (the rejected one) was adversely affected by events occurring before the fpd was initiated. This is a good example of how difficult it

Fig. 17. Plot of the natural logarithm of the envelope of a freee precession decay tail together with the least-squares fit. In this particular case initial B_{mo} = 3.97 microgauss, and T_2 = 23 min.

Fig. 18. T_2 of the free precession decay tails for three different values of the initial B_{mo}.

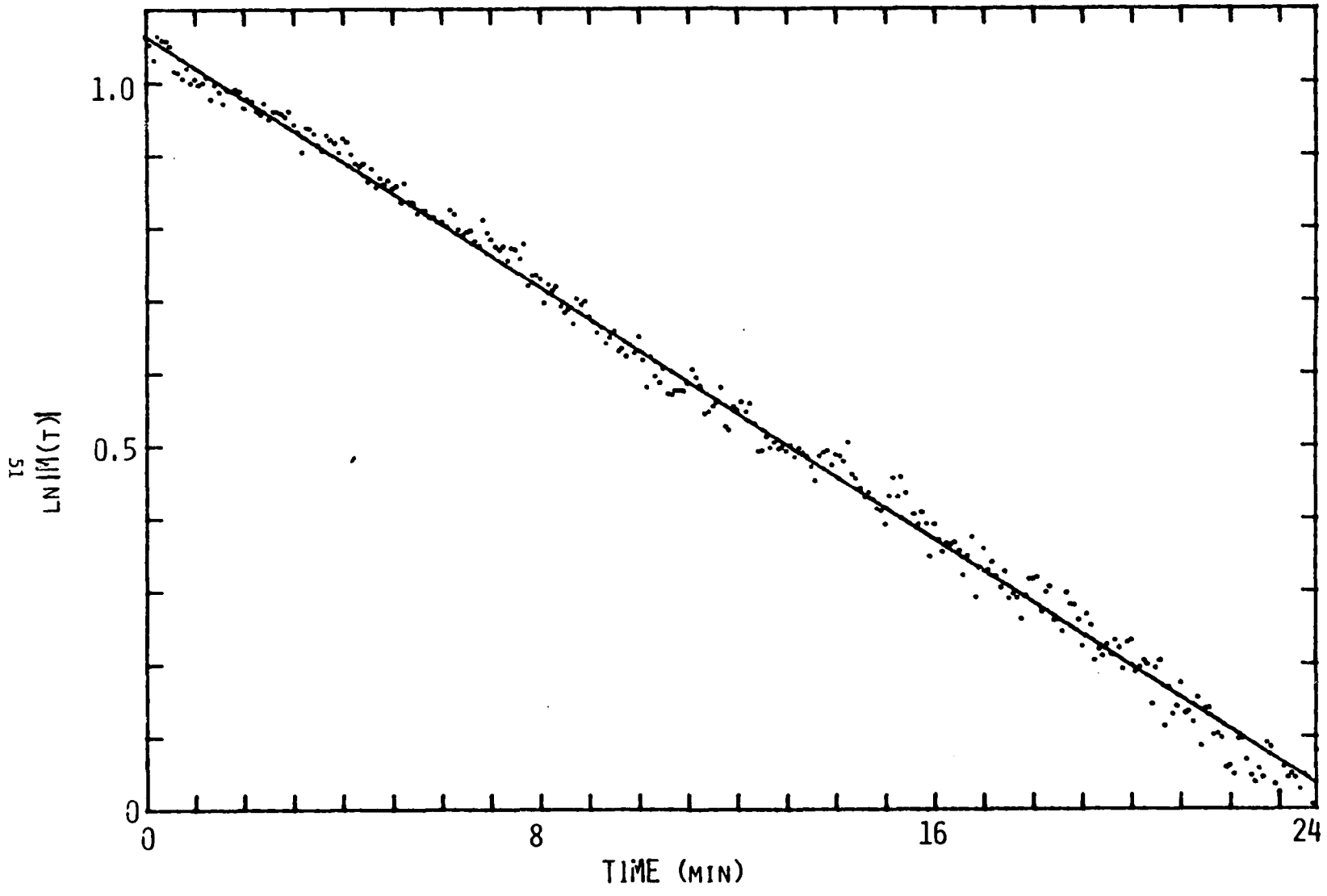

Fig. 16

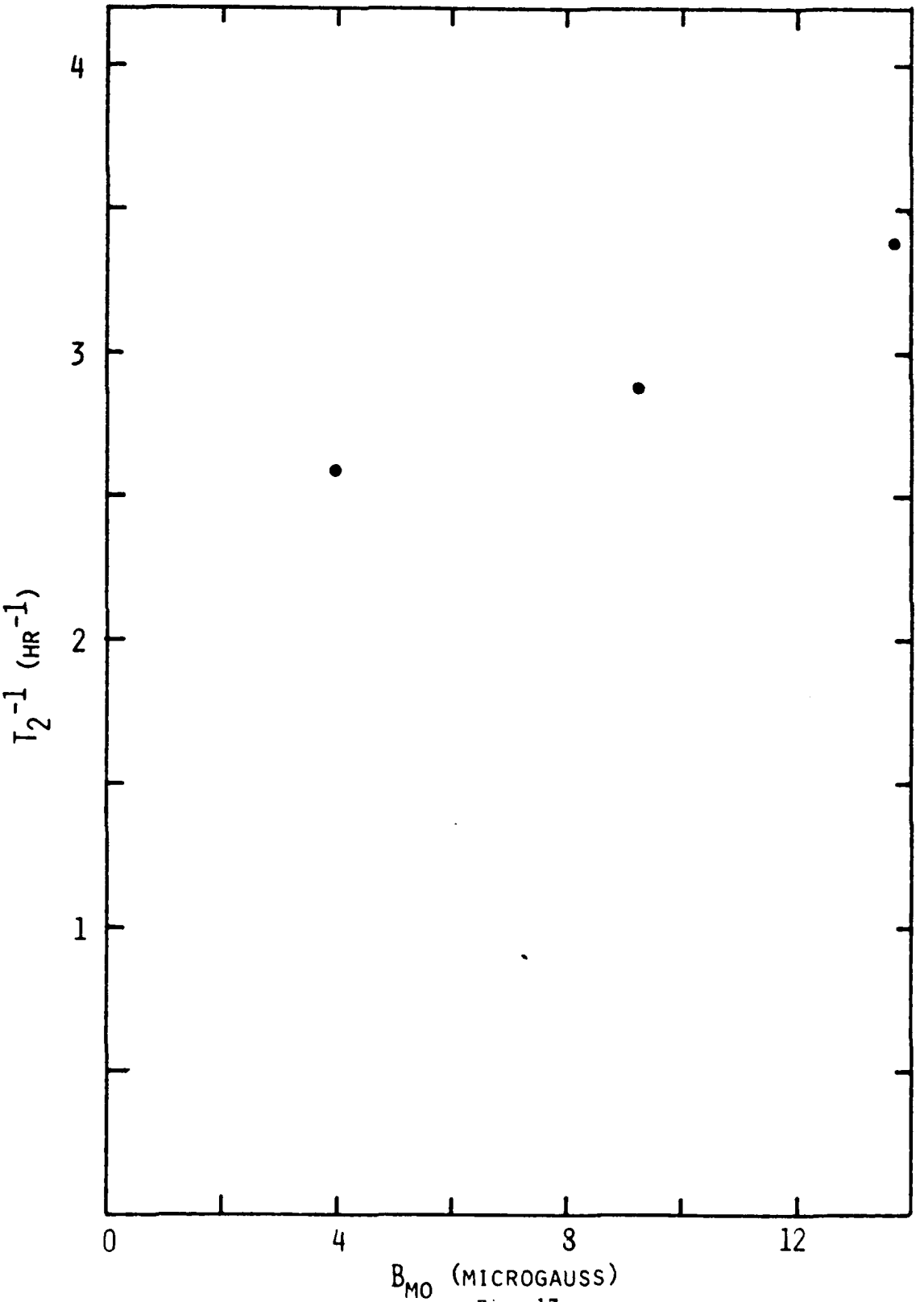

Fig. 17

is to obtain understandable transverse decay results from liquid mixtures where inhomogeneities in the sample magnetization take a long time to dissipate.

e. Measurements made on a Gas Mixture Sample

There were two reasons to try using a He^3-He^4 gas mixture despite the known deficiencies of the sample cell. The first is that the He^3 diffusion coefficient could be expected to be an order of magnitude or more larger in the gas than in the liquid. (The ratio of He^4 liquid density at 4.2 K to that of the saturated vapor is approximately 7.5). Thus the use of a gas mixture should help answer the question of whether the liquid mixtures were approaching motional narrowing. The second reason was to determine whether the reduced amount of He^4 would increase the loss of He^3 polarization during the sample cell filling process. This issue is of interest because the new precision gyro apparatus is designed to be used with gas mixtures. Because of this latter issue, the amount of He^4 chosen for these measurements was that necessary to produce a final pressure slightly less than one atmosphere. This is the maximum amount of He^4 that can be used without forming liquid in the sample cell. It should also be noted that the He^3 density will be lower in a gas mixture than in a liquid mixture. The ratio of He^3 concentration in He^4 vapor at 4 K to that in the liquid is 1.4 to 1. This effect, however, is overwhelmed by the much greater density of the liquid compared to that of the vapor with the net result that the He^3 density in the liquid is approximately five times that in the gas.

We now summarize the results that were anticipated in the gas mixture measurements:

1) The magnetization should be reduced to 30% of the liquid value (everything else being equal) because of the lower He^3 density if the reduced amount of He^4 does not adversely affect the relaxation of He^3 during the sample cell filling process.

2) T_1 might well decrease because the reduced He^4 density could increase the efficiency of wall-induced relaxation. There is insufficient information to judge how the gradient-induced relaxation rate would change.

3) Despite a possible decrease in T_1 it is expected that the transverse decay time should increase for two reasons: a) reduction in magnetization will yield a smaller cell-shape-induced gradient, and b) the more rapid diffusion will cause motional narrowing.

In one experimental run we were able to make one T_1 measurement at 61.7 μG and a sequence of free precession decay measurements in exactly the same fashion described for the liquid mixture. The initial magnetization was reasonably within expectation. The initial magnetization yielded $B_{mo} \simeq 9$ μG which is about 20% of the value obtained in a fairly comparable liquid mixture run. Since we had expected a 30% factor, this is an indication that the reduced amount of He^4 may have led to a somewhat less efficient transfer of polarized He^3 from the optical pumping cell to the sample cell. This effect, however, does not appear to be large enough to cause concern about the viability of future gas mixture work using these techniques.

The T_1 measurement yielded a relaxation time of 2.7 hours. This is a factor of seven less than would be expected for a liquid sample in a field of 61.7 μG. As was the case with the liquid mixture, it is fairly certain that the T_1 was dominated by surface effects, that is, wall-induced relaxation and superficial magnetic dipole gradients. Thus as we have previously noted, the T_1 in the precision gyro apparatus should be significantly longer because a much larger cell with a solid H_2 coating will be used.

Although the magnetization and T_1 measurements in the gas mixture were not very surprising, this was not true of the transverse decay measurements. These measurements were made and analyzed using virtually the same techniques as were

used before. Both discrete Fourier transform and envelope decay analysis are shown in Figs. 18-23. The most remarkable of these lineshape plots are those obtained with B_o in the $\pm$ z direction (Figs. 18, 19). These two lineshapes are distinctly bimodal in character, suggesting that there were two separate regions in the cell with different Larmor frequencies. Note, however, that the remaining lineshapes which resulted when B_o was in a horizontal direction are very narrow with little or no indication of a secondary or satellite peak. The only exception to this was the first measurement made with a horizontal field (Fig. 20) which shows a slight shoulder indicating the possibility of an unresolved secondary peak.

There appears to be only one straightforward explanation for these somewhat peculiar results. That is that there was slightly too much He^4, and a small fraction of the sample cell (the data suggest ~ 10%) contained liquid mixture rather than gas. The liquid portion would have a magnetization approximately five times that of the gas part and would have the shape of a rather aspheric puddle in the bottom of the sample cell. These two factors mean that the Larmor frequency of the liquid portion of the sample cell would be shifted from that of the gas part by an amount proportional to the average sample magnetization. (See ref. 4 for a detailed discussion of the effect of sample shape on the Larmor frequency). This is exactly what was observed in the vertical field measurements where a 34% decrease in the average sample magnetization was accompanied by a 32% decrease in the splitting between the peaks. (The fact that the satellite peak shifted from one side of the primary peak to the other is consistent with the fact that B_o was reversed between measurements while the magnetization was not.)

Figs. 18-23. Fourier transforms of free precession decays (lineshape functions) of a nominal gas mixture (see text) as a function of initial $B_{ml} = 8\pi\bar{M}/3$ where $\bar{M}$ is the average sample magnetization.

Fig. 18. Both $\vec{B}_o$ and $(B_{mo})_z$ in $\pm$ z direction.

Fig. 19. $\vec{B}_o$ in - z direction and $(B_{mo})_z$ in + z direction.

Fig. 20. $\vec{B}_o$ in -y direction and $(B_{mo})_y$ in + y direction.

Figs. 21-23. Both $\vec{B}_o$ and $(B_{mo})_y$ in + y direction.

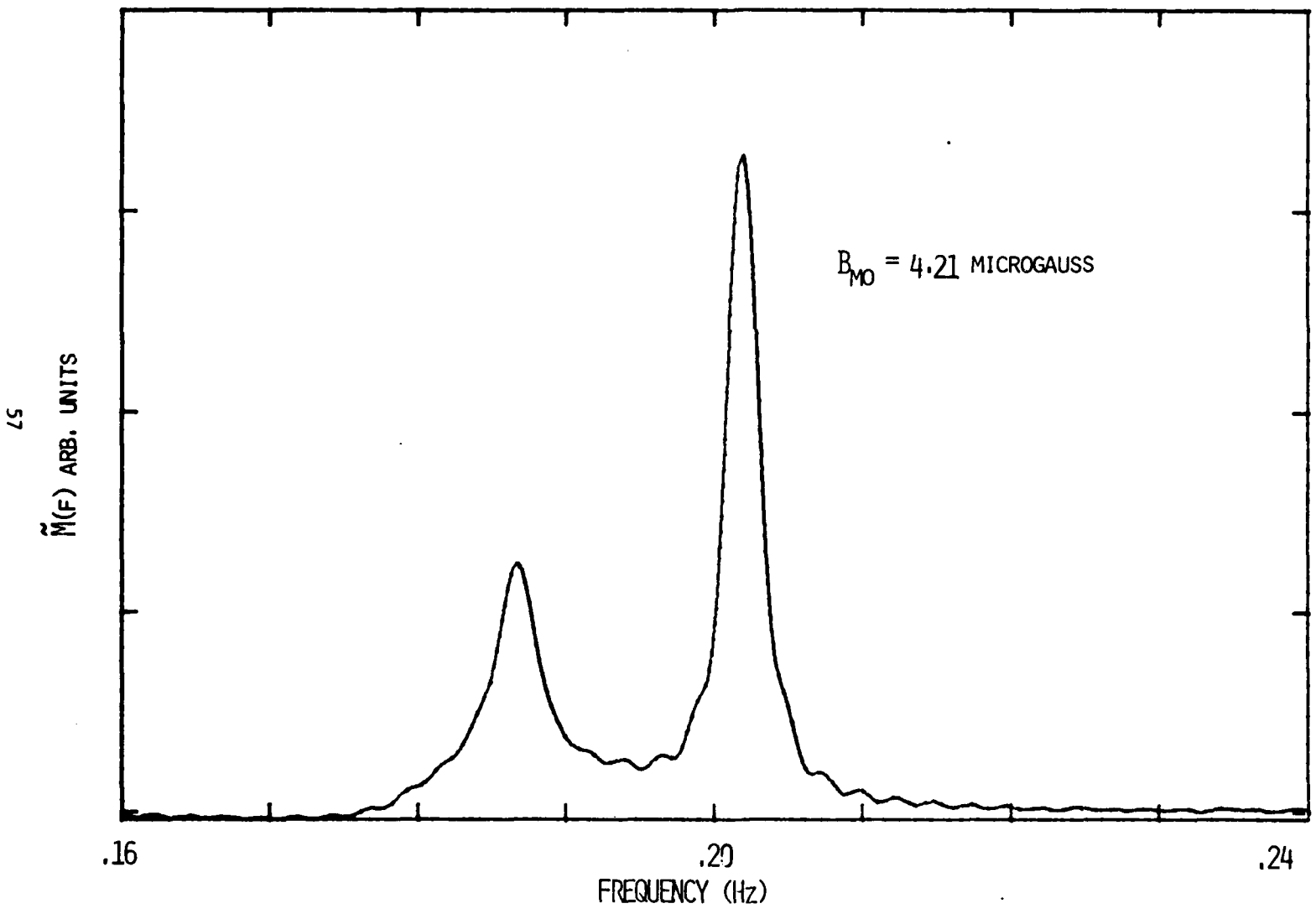
B_{MO} = 4.21 MICROGAUSS
$\tilde{M}(F)$ ARB. UNITS
.16
.20
.24
FREQUENCY (Hz)

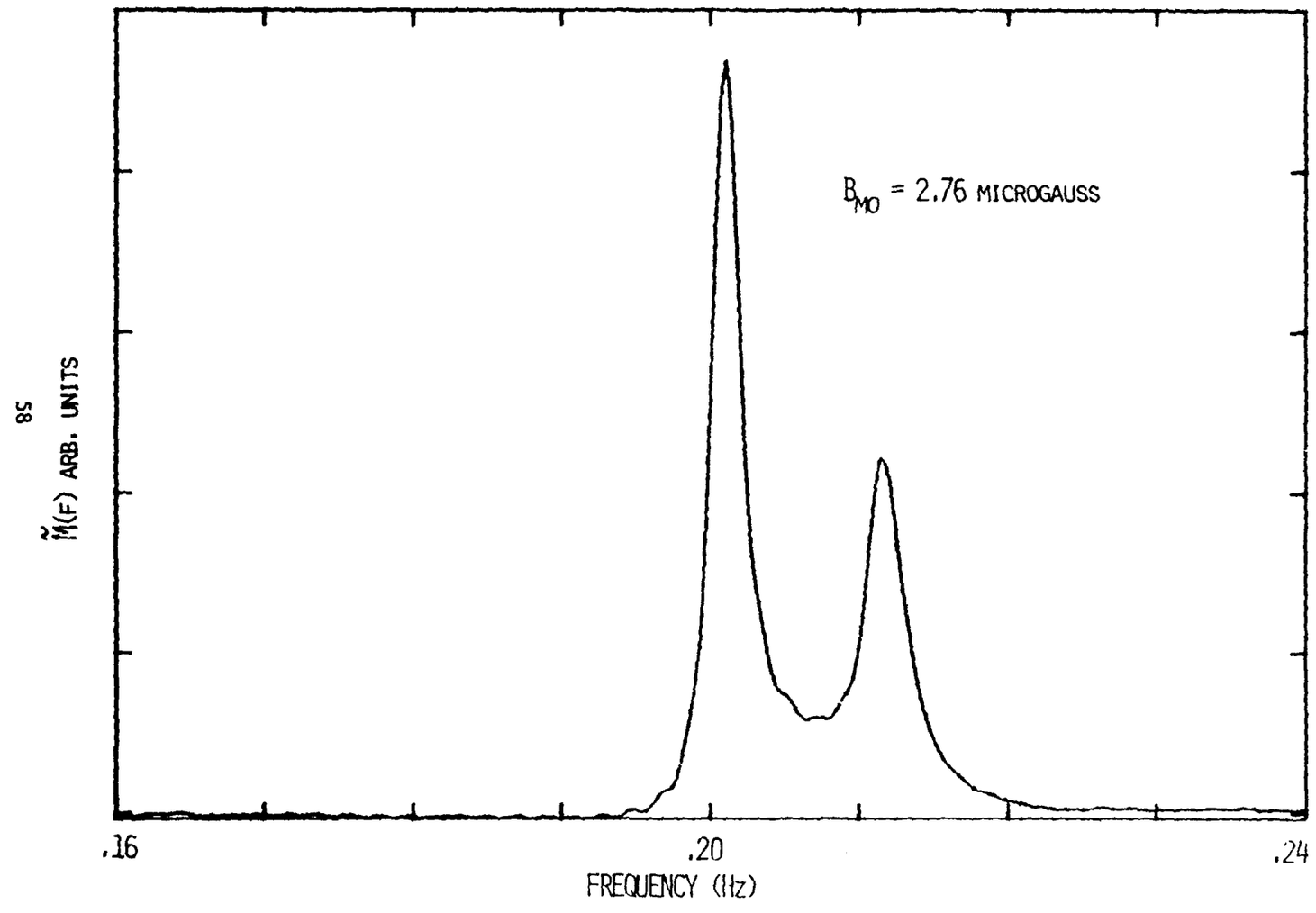
B_{MO} = 2.76 MICROGAUSS
85
$\tilde{M}(F)$ ARB. UNITS
.16
.20
.24
FREQUENCY (Hz)

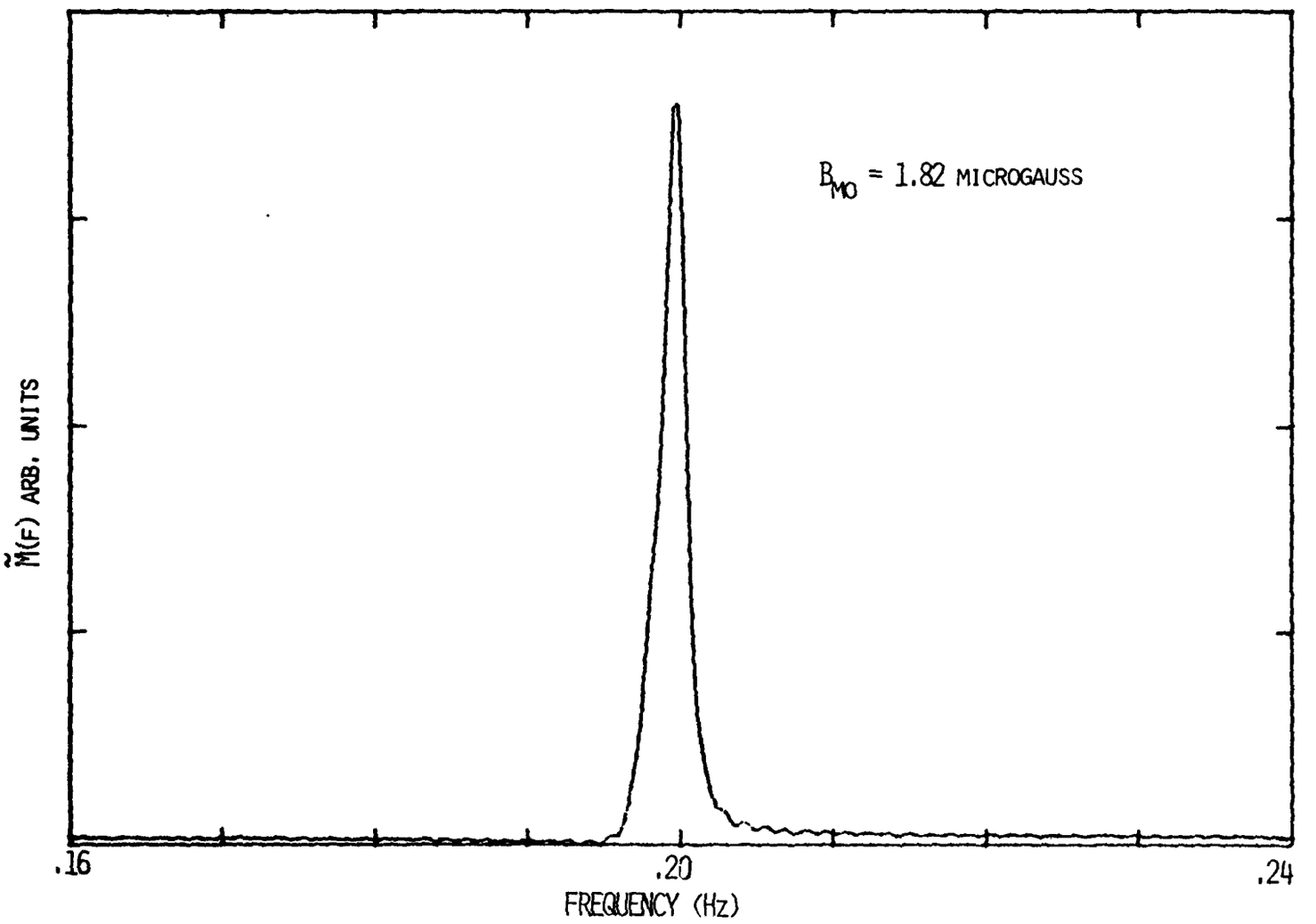
B_{MO} = 1.82 MICROGAUSS
$\tilde{M}(F)$ ARB. UNITS
.16
.20
.24
FREQUENCY (Hz)

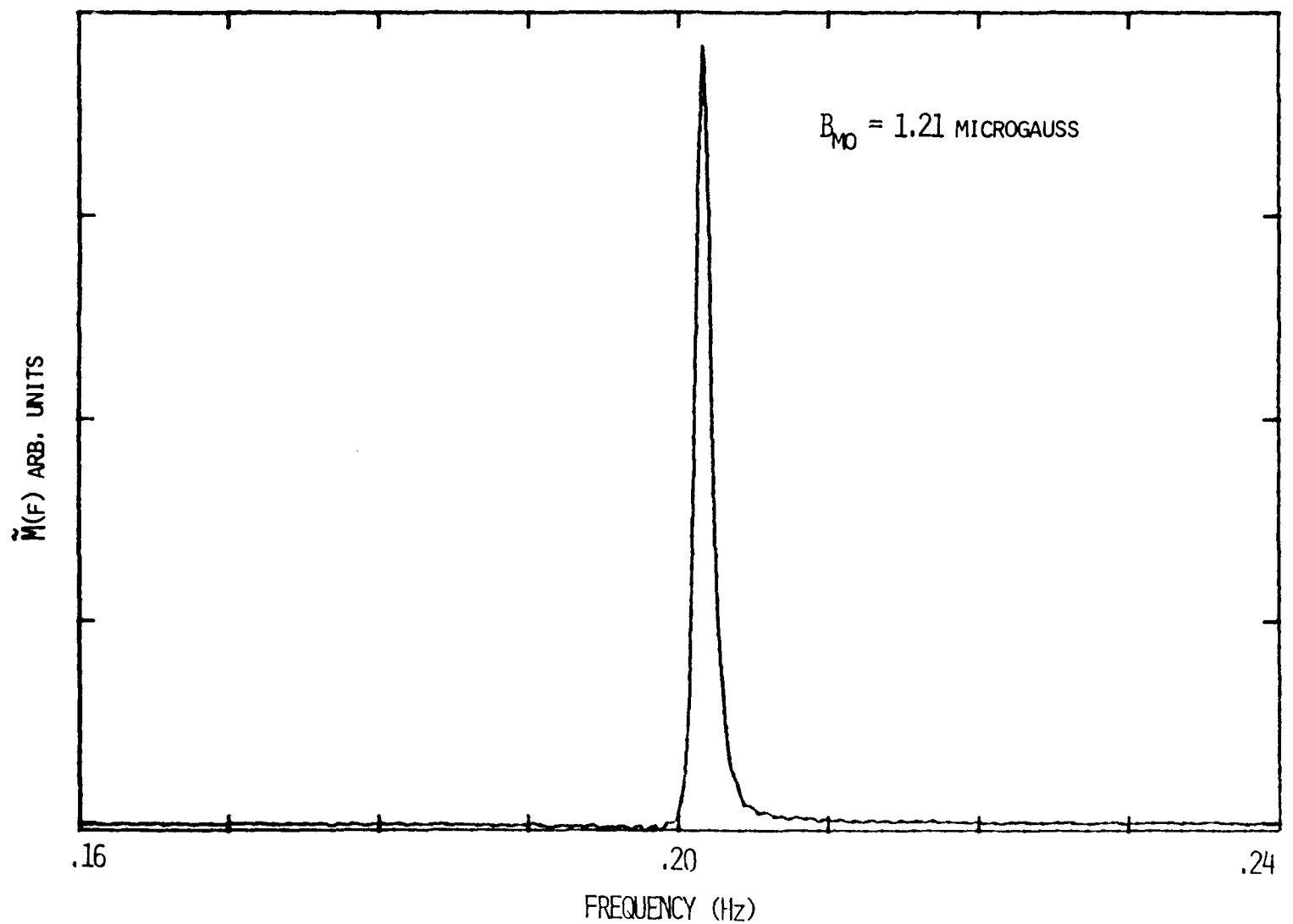
B_{MO} = 1.21 MICROGAUSS
$\tilde{M}(F)$ ARB. UNITS
.16
.20
.24
FREQUENCY (Hz)

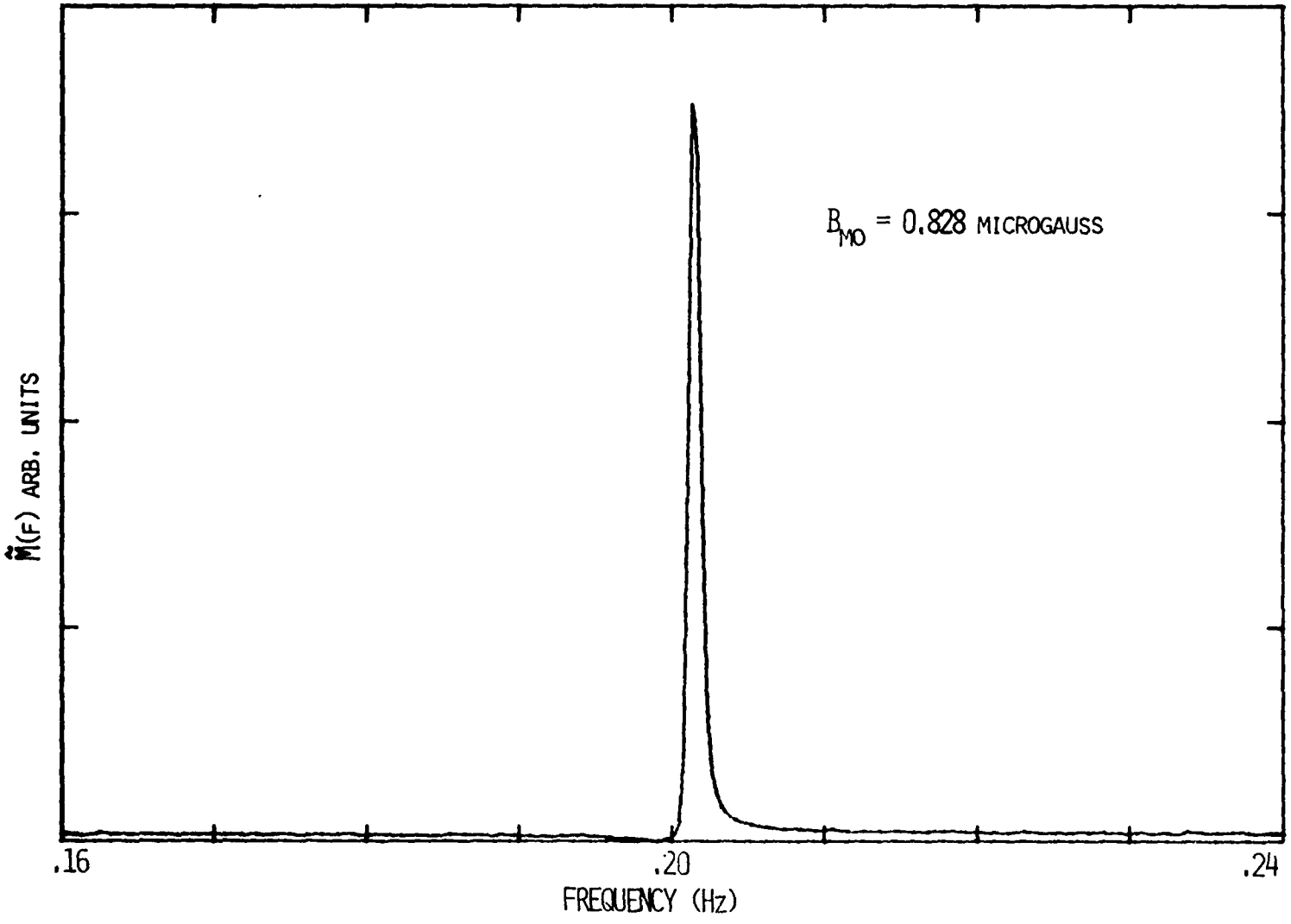

T9

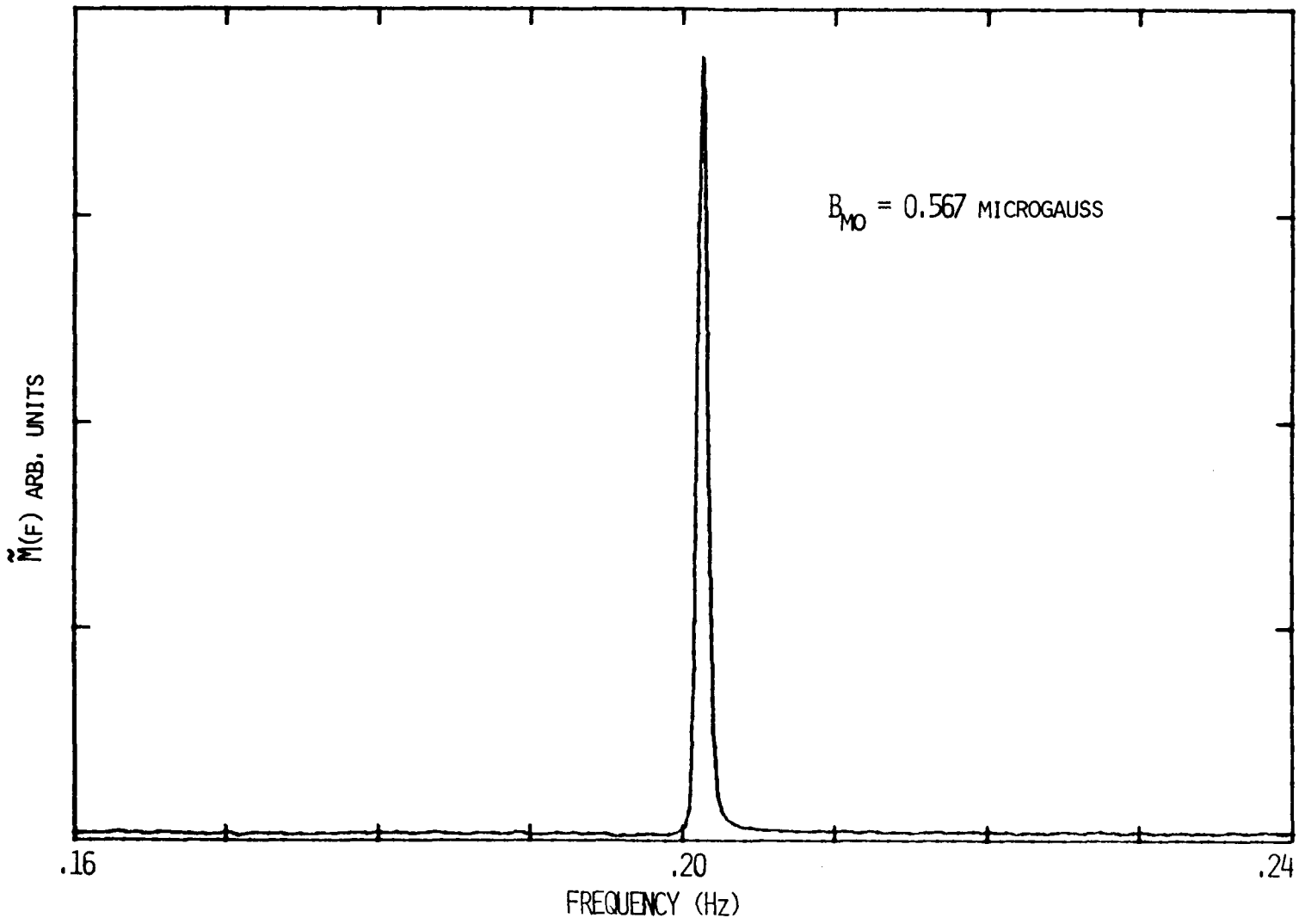
B_{MO} = 0.567 MICROGAUSS
$\tilde{M}(F)$ ARB. UNITS
.16
.20
.24
FREQUENCY (Hz)

An attempt to model this proposed explanation by considering the liquid portion of the sample to be an oblate spheroid located adjacent to a spherical gas sample yielded qualitatively correct results. Quantitatively, however, the agreement was not totally convincing. In particular the model predicted a ~40% larger splitting than that observed for a vertical $\vec{B}_o$. Additionally, although the model correctly indicates that the splitting should be smaller for a horizontal $\vec{B}_o$, it also indicates that it should be readily resolvable for the larger magnetization values. It should be noted, however, that this model is rather crude and has at least one major defect: the exchange of He^3 atoms between the two sample regions has been entirely ignored. The effect of such exchange would be to tend to fuse the two peaks into one broader one.

Thus, while the identification of the bimodel lineshape of the vertical precession data with a liquid-gas phase separation is not definitive, there is sufficient reason to be cautious in drawing conclusions from this data. In spite of this limitation, an envelope decay analysis was performed on all of the free precession decay measurements made with a horizontal $\vec{B}_o$. Of these the last three (corresponding to Figs. 21-23) were accurately fit by a simple exponential decay. If in fact there were liquid-gas phase separation, this would indicate that for these weak magnetizations the exchange of He^3 atoms between liquid and vapor was sufficiently rapid to completely wash out the difference in Larmor frequencies between the two phases. In any case, it was found that the exponential decay rate (T_2^{-1}) varied as the <u>square</u> of the mean sample magnetization with the longest measured time constant being 33 minutes. This is exactly the kind of dependence that would be expected if the transverse decay were controlled by the rapid exchange of spins between two regions of slightly differing Larmor frequencies. It is also, however, what would be expected if the transverse relaxation were dominated by a field gradient arising from sample-shape asphericity.

Because of the possibility of liquid-gas phase separation it is not possible to draw any firm conclusions by making comparisons with the liquid-mixture transverse decay times. It should be noted, nevertheless, that with the exception of the 33 min. decay time (the longest that we have observed) the transverse decay times of the gas (or gas/liquid) mixture were shorter than those of the liquid mixture, despite the fact that all the magnetizations used in the former measurements were less than those in the latter.

V. Summary and Conclusions

In summary, progress has been achieved in the following four areas:

a) A new ultra-low magnetic field shield has been established which achieved a field of 2×10^{-8} G over a substantial volume. This not only exceeds our requirements, but to the best of our knowledge is the lowest absolute magnetic field region ever made.

b) The precision fused quartz gyro housing has been received and is ready for final tumble-lapping, shield deposition, and assembly procedures. The new cryostat probe is in the construction phase.

c) The engineering Ph.D. thesis of Capt. Gerald Shaw which analyzes several aspects of the dynamic behavior of our nuclear gyro has been completed.

d) Our original experimental apparatus was modified and run four more times (once with a nominal gas mixture) with the result of achieving an exponential decay characteristic in the limit of a small magnetization and a significant reduction in the magnetic contaminant problem. This has had the effect of increasing the transverse decay time by over an order of magnitude over what we had previously observed. The data indicated that the transverse decay times were strongly affected, if not dominated by sample-induced gradients.

The improvement achieved with the modification of our original apparatus has made clear the impact of the sample shape on the transverse decay time and has convinced us of the importance of using gas mixtures in a precision sample cell made out of high grade material. Since these are features of the new apparatus, we feel that if the blown Pyrex cell worked as well as it did, we have every expectation that the new apparatus will achieve the conditions necessary for quality gyro performance.

REFERENCES

1. See, for example, A. Abragam, *The Principles of Nuclear Magnetism* (Oxford University Press, Oxford, 1961).
2. The possibility that there may be an electric dipole has generated a great deal of interest since its existence would be a manifestation of time reversal invariance. Because of its extremely small size, its possible existence does not affect our present considerations.
3. The need for some of these requirements may not be obvious but will become clearer later in the discussion. Details are found in ref. 4.
4. M. A. Taber, Ph.D. Thesis, Stanford University, 1978.
5. B. Cabrera, Ph.D. Thesis, Stanford University, 1975.
6. F. D. Colegrove, L. D. Schearer, and G. K. Walters, Phys. Rev. 132, 2561 (1963).
7. R. Barbé, F. Laloë, and J. Brossel, Phys. Rev. Lett. 34, 1488 (1975).
8. J. Clarke, W. M. Goubau, and M. B. Ketchen, J. Low Temp. Phys. 25, 99 (1976). The noise characteristics of the dc SQUID reported in this reference are somewhat better than those of commerically available rf-biased SQUIDs but have the disadvantage of requiring custom laboratory fabrication.
9. I. Oppenheim and M. Bloom, Can. J. Phys. 39, 845 (1961).
10. R. Barbé, M. Leduc, and F. Laloë, J. Phys. (Paris) 35, 699 (1974). This subject is also reviewed in ref. 4.

11. Cabrera (ref. 5) has measured the remanent magnetization at 4 K of a number of materials that are useful for cryogenic applications. These measurements were done with a SQUID magnetometer. He found that many materials are ferromagnetically contaminated, but that some (e.g., synthetic fused quartz, and 6061 aluminum) had undetectably small remanent magnetization. We assume that materials that pass this test are acceptable for the He^3NG, but this remains to be proven.

12. Relaxation time measurements of pure He^3 gas at 4.2 K in a bare Pyrex cell have been reported by R. Chapman and M. G. Richards, Phys. Rev. Lett. 33, 18 (1974).

13. G. K. White and J. A. Birch, Phys. Chem. Glasses 6, 85 (1965).

14. See, for example, E. A. Lynton, *Superconductivity* (Methuen and Co., Ltd., London, 1969), 3rd ed.

15. B. W. Maxfield, and W. L. McLean, Phys. Rev. 139, A1515 (1965).

16. It is likely that the average drift reported by CGK over a 20 hour period is mostly not due to any true, long-term drift. In fact, CGK suggested that what was observed was largely due to the effect on the SQUID electronics of the decline in the liquid He level in their dewar. They further suggest that improvements in the SQUID electronics could reduce the drift due to this source.

17. This can be accomplished by suddenly switching the magnetic field direction by 90^o. Accurately constructed field coils that are orthogonal to those providing $\vec{B}_o$ would be included in the gyro case to allow this capability.

18. F. London, *Superfluids* (Dover, New York, 1961) Vol. I.

19. H. Hellwig, *Proc. 28th Annual Symposium on Frequency Control* (Elec. Ind. Assoc., Washington, D.C., 1974).

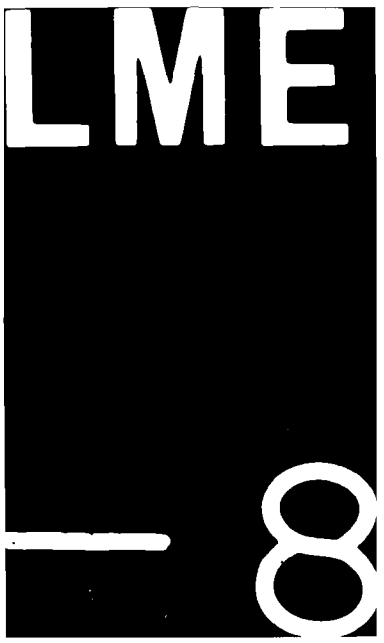
LME
8